Cholesterol-mediated Lysosomal Dysfunction in *APOE4* Astrocytes Promotes α-Synuclein Pathology in Human Brain Tissue

Louise A. Mesentier-Louro[1-6,13], Camille Goldman[1-6,13], Alain Ndayisaba[6-9], Alice Buonfiglioli[1-5], Rikki B. Rooklin[1-5], Braxton R. Schuldt[1-5], Abigail Uchitelev[1-5,12], Vikram Khurana[6-11], Joel W. Blanchard[1-6,14, *]

1. Icahn School of Medicine, Mount Sinai, New York, NY, USA
2. Nash Family Department of Neuroscience, Mount Sinai, New York, NY, USA
3. Friedman Brain Institute, Mount Sinai, New York, NY, USA
4. Ronald M. Loeb Center for Alzheimer's Disease, Mount Sinai, New York, NY USA
5. Black Family Stem Cell Institute, Mount Sinai, New York, NY, USA
6. Aligning Science Across Parkinson's (ASAP) Collaborative Research Network, Chevy Chase, MD 20815, USA
7. Ann Romney Center for Neurologic Diseases, Brigham and Women's Hospital, Boston, MA, USA
8. Division of Movement Disorders, American Parkinson Disease Association (APDA) Center for Advanced Research and MSA Center of Excellence, Department of Neurology, Brigham and Women's Hospital, Boston, MA, USA
9. Harvard Medical School, Boston, MA, USA
10. The Broad Institute of MIT and Harvard, Cambridge, MA, USA
11. Harvard Stem Cell Institute, Cambridge, MA, USA
12. Macaulay Honors College at Hunter College, New York, NY, USA
13. These authors contributed equally
14. Lead contact

*Correspondence: joel.blanchard@mssm.edu

Summary

The pathological hallmark of neurodegenerative disease is the aberrant post-translational modification and aggregation of proteins leading to the formation of insoluble protein inclusions. Genetic factors like *APOE4* are known to increase the prevalence and severity of tau, amyloid, and α-Synuclein inclusions. However, the human brain is largely inaccessible during this process, limiting our mechanistic understanding. Here, we developed an iPSC-based 3D model that integrates neurons, glia, myelin, and cerebrovascular cells into a functional human brain tissue (miBrain). Like the human brain, we found pathogenic phosphorylation and aggregation of α-Synuclein is increased in the *APOE4* miBrain. Combinatorial experiments revealed that lipid-droplet formation in APOE4 astrocytes impairs the degradation of α-synuclein and leads to a pathogenic transformation that seeds neuronal inclusions of α-Synuclein. Collectively, this study establishes a robust model for investigating protein inclusions in human brain tissue and highlights the role of astrocytes and cholesterol in *APOE4*-mediated pathologies, opening therapeutic opportunities.

Keywords:

α-Synuclein; iPSC-derived brain model; Lewy Body Dementia; Alzheimer's Disease; Astrocytes; *APOE4*; Lysosomal dysfunction; Cholesterol metabolism; Neurodegeneration; miBrain.

Introduction.

Alzheimer's disease (AD) is canonically associated with amyloid-β and tau pathology[1]. However, neuronal intracellular inclusions of aggregated α-synuclein (α-Syn) are present in 50-90% of AD cases[2-5]. Phosphorylated α-Syn often aggregates forming Lewy Bodies and Lewy neurites, which are frequently found in the brains of individuals with AD[2-4]. The occurrence of α-Syn inclusions with amyloid-β and tau exacerbates neurodegeneration particularly in brain regions associated with memory and executive functions[5-10]. Indeed, clinical studies show that AD patients with α-Syn pathology exhibit faster cognitive decline compared to those with only amyloid-β and tau pathology[11,12]. The strongest genetic risk factor for late-onset AD, *APOE4*, significantly increases both the prevalence and severity of α-Syn pathology in AD[12,13] and is one of the most well replicated genetic risk factors for Lewy Body Dementia (LBD)[14,15]. However, the mechanisms by which genetic factors like *APOE4* influence the presence and severity of α-Syn pathology are largely unclear. Insight into the mechanisms underlying non-amyloid-β co-pathologies could lead to much needed therapeutic and diagnostic opportunities in AD and LBD.

The development of model systems that faithfully recapitulate α-Syn pathology and the genetic and environmental context of the human brain is essential to uncovering how ancillary genetic factors, such as APOE4, modify α-Syn-driven neurodegeneration. Addition of pre-formed fibrils (PFFs) of α-Syn are commonly employed in mice[16,17] and *in vitro* models[18-20] to induce α-Syn pathology. PFFs are reported to spread across the brain in a prion-like manner corrupting endogenous α-Syn and promoting the propagation of pathology[18,21,22]. However, animal models and *in vitro* systems with α-Syn PFFs are plagued with high variability and often fail to induce phosphorylated α-Syn-rich inclusions while having significant biohazards concerns from the use of prion-like particles[23]. This highlights the need for more physiological models that do not rely on PFFs and can explore multicellular mechanisms of disease. For instance, the induction of neurodegenerative phenotypes in cells cultured in traditional two-dimensional (2D) conditions may be limited by a chemical and mechanical microenvironment that is vastly different from *in vivo* conditions[24]. In contrast, three-dimensional (3D) *in vitro* systems have proven more efficient than 2D systems at replicating key pathological features such as amyloid-β plaques and tau tangles[25,26]. Combining genetic approaches with 3D tissue engineering is a promising alternative for developing more physiological models of neurodegenerative disease.

We recently developed the human **m**ulti-cellular **i**ntegrated **Brain** (**miBrain**), a fully induced pluripotent stem cell (iPSC)-derived 3D human brain tissue that incorporates neurons, glia, and microvasculature into an anatomically precise tissue capable of modeling neurodegeneration in a dish[27]. The miBrain is an *in vitro* human brain tissue containing the major cells and tissues found in human brain tissue including a blood-brain barrier, active neurons with oligodendrocytes, and the brain immune cells- such as microglia and astrocytes. The miBrain can be generated from patient-derived iPSCs. Because it is an engineered tissue, this permits the generation of genetically mixed tissue. For example, coupled with CRISPR-edited iPSC lines, we can generate genetically identical miBrains with AD risk genes such as *APOE4* in specific cell types. We have developed methods to model neuropathological phenotypes associated with amyloid-β and tau in the miBrains[27]. Here, we expanded the miBrain technology, by first developing methods to cryopreserve the miBrain, enabling the production of large batches of full or partial miBrains and dramatically reducing the batch-to-batch variability and improving scalability of the model system. Leveraging this advanced approach, we developed the first highly reproducible model of α-Syn neuropathological phenotypes in an iPSC-derived human brain tissue. We then apply the miBrain to investigate the mechanisms by which *APOE4* promotes increased α-Syn phosphorylation and aggregation in human brain tissue. Our results revealed that *APOE4* increases α-Syn phosphorylation and neuronal inclusions via non-cell-autonomous mechanisms driven by lipid accumulation in APOE4 astrocytes. Our results establish robust methods for modeling α-synuclein

pathological phenotypes in human brain tissue and highlight a causal role of astrocytes and lipids in *APOE4*-mediated α-Syn pathologies, opening new therapeutic opportunities AD, LBD, and other neurodegenerative diseases.

Results

Induction of α-Syn intracellular inclusions in a multi-cellular integrated Brain (miBrain) tissue.

Intracellular neuronal inclusions of phosphorylated and aggregated α-Syn have been challenging to reproduce in human brain cells or tissue, typically requiring very long maturation protocols[28] and the concomitant use of PFFs[29]. Therefore, we sought to develop a robust, high-fidelity model of α-Syn intracellular inclusions leveraging the multi-cellular integrated Brain (miBrain). The miBrain is a human brain tissue generated by encapsulation of iPSC-derived neurons[29,30], astrocytes[31,32], endothelial cells[33-36], mural cells[33,37], oligodendrocyte precursor cells (OPCs)[38], and microglia[39]. miBrains displayed homogenous TUJ1$^+$ neuronal networks and PECAM1$^+$ vascular structures (**Fig. 1a**). Staining for multiple markers revealed interactions and co-localization between S100β$^+$ and AQP4$^+$ astroglia and PECAM1$^+$ vascular structures, vascular coverage with NG2$^+$ mural cells, myelin basic protein (MBP)$^+$/neurofilament$^+$ neuro-myelin structures, and the presence of IBA1$^+$ microglia in a grid-like pattern (**Fig. 1b**), consistent with the specific cell types encapsulated in the miBrain. In other platforms such as brain organoids, significant variability in cell composition have been reported, leading to a high-degree of experimental variability and consistency[40]. Therefore, to minimize miBrain batch-to-batch variability and increase the scalability of the miBrain, we developed methods to cryopreserve large batches of miBrain tissue containing multiple cell types at a defined ratio. Off-the-shelf cryopreserved miBrains retain more than 90% cell viability upon thaw and expressed specific cell markers two weeks after thawing into the 3D culture system (**Extended Data Fig. 1a, b)**. The ratio of neurons to nuclei did not significantly differ between three different batches of thawed miBrain tissue ($p = 0.29$, **Extended Data Fig. 1b**).

Phosphorylation of α-Syn on S129 is the predominant pathological modification associated with α-Syn aggregation and neuronal inclusions, and, therefore, is an established method for detecting pathogenic transformation of α-Syn[41,42]. Consequently, we first investigated whether the conventionally employed α-synuclein PFFs[16-20] can increase phosphorylated α-Syn (p-Syn) in the miBrains. Inoculating the miBrain culture media with α-Syn PFFs significantly increased p-Syn levels when compared to control miBrains ($p = 0.0175$, **Extended Data Fig. 1c**), indicating the suitability of the tissue to develop α-Syn pathological phenotypes. However, using this approach, p-Syn was mostly seen as dispersed puncta (**Extended Data Fig. 1c**) rather than within the typical neuronal inclusions that are hallmarks of synucleinopathies[43]. In addition, there was a high degree of variability in the presence and abundance of p-Syn (**Extended Data Fig. 1c**) consistent with other reports comparing the pattern of α-Syn aggregate spreading in PFF models across different research groups[17]. Therefore, we sought to identify more robust methods for inducing pathogenic α-Syn phenotypes in the miBrain.

A recent study found that iPSC-derived neurons express low levels of the gene encoding α-Syn (*SNCA)* compared to adult human brain tissue and, therefore, used *SNCA* overexpression to increase α-Syn to physiological levels and induce its phosphorylation and neuronal inclusions[29]. Thus, to achieve brain-like levels of *SNCA* and induce pathological phenotypes, we generated neurons from iPSCs with inducible expression of *SNCA* bearing the A53>T mutation (A53T), known to increase α-Syn's aggregation propensity[29,44,45]. SNCA-A53T was fused to a small folding green fluorescent protein (sfGFP, diagram in **Fig. 1c**), enabling live imaging and direct visualization of α-Syn accumulation[46]. We confirmed that α-Syn phosphorylation is dependent on the α-Syn protein non-amyloid component (NAC) domain and not

influenced by sfGFP (**Extended Data Fig. 1d**). In 2D monocultures, wild-type (WT) and A53T neurons have similar levels of p-Syn, which significantly increased in A53T neurons with the addition of PFFs (**Extended Data Fig. 1d**). In contrast, in the absence of exogenously added PFFs, miBrains with A53T neurons already showed a significant increase in neuronal p-Syn compared to isogenic miBrains harboring WT neurons ($p = 0.0007$), suggesting that the more physiological 3D environment of the miBrain is more permissive to α-Syn pathology. We found the addition of PFFs in A53T miBrains further increased p-Syn levels compared to WT miBrains with PFFs ($p < 0.0001$) and A53T miBrains without PFFs ($p = 0.038$, **Fig. 1c**). The SNCA-A53T-sfGFP signal co-localized with p-Syn (**Fig. 1d** and **Supplementary Video 1**; Control: 13.54% ± 2.37, PFFs: 17.79% ± 2.61, mean of the percentage of colocalization ± SEM, n = 4), indicating that SNCA-A53T undergoes phosphorylation at a similar extent with or without PFFs ($p = 0.27$, unpaired t-test). Although most of the p-Syn co-localized with sfGFP (Control: 86.7% ± 1.9, PFFs: 88.0% ± 1.4, n = 4), we also found p-Syn that did not co-localize with sfGFP (Control: 13.3% ± 1.9, PFFs: 12.0% ± 1.4, n = 4), indicating that endogenous, non-A53T α-Syn is also phosphorylated. This data shows that A53T miBrains developed p-Syn-rich inclusions via corruption of both induced (A53T) and endogenous (WT) α-Syn without requiring the use of PFFs.

In the human brain, lipid droplets[47] and mitochondria[48] are frequently observed within α-Syn$^+$ inclusions. In A53T miBrains, the neutral lipid marker Lipid Spot overlapped with SNCA-A53T-sfGFP and with p-Syn (**Fig. 1e)**. The co-localized volume between Lipid Spot and p-Syn was significantly increased ($p = 0.02$) in A53T miBrains compared with WT (**Fig. 1e**), consistent with previous reports on p-Syn$^+$/Lipid Spot$^+$ neurotoxic inclusions in iPSC-derived neurons[29]. Furthermore, the volume of aggregated α-Syn overlapping with mitochondrial marker Tom20 was significantly increased in A53T miBrains compared to WT miBrains ($p = 0.04$, **Extended Data Fig. 1e**), consistent with reports of aggregated α-Syn bound to mitochondria in α-Syn$^+$ inclusions in the human brain[49].

Neuronal inclusions of α-Syn present as spherical dense Lewy Bodies, less dense “pale bodies”, and Lewy neurites that can be thread-like or attain a varicose appearance[43]. Through serial live imaging, we observed somatic and neuritic presentations of the SNCA-A53T-sfGFP signal in miBrains, resembling various morphological presentations found in the human brain (**Fig. 1f, i-iii**). During the first 12 weeks, there was a significant increase in the number of α-Syn somatic inclusions (2 weeks: $4.7 \times 10^{-5} \pm 1.9 \times 10^{-6}$, 12 weeks: $8.5 \times 10^{-5} \pm 4.0 \times 10^{-6}$, number of sfGFP$^+$ inclusions normalized by total sfGFP volume, $p < 0.0001$, unpaired t-test), and no significant changes in the number of α-Syn neuritic inclusions (2 weeks: $1.5 \times 10^{-7} \pm 4.4 \times 10^{-8}$, 12 weeks: $3.4 \times 10^{-7} \pm 1.6 \times 10^{-7}$, $p= 0.3$; **Fig. 1f**). *In vivo* aggregation of α-Syn within neuronal inclusions promotes neuronal death[50,51]. Soluble biomarkers of cell death (lactate dehydrogenase (LDH)) were significantly higher in media of A53T miBrains compared to WT miBrains ($p = 0.0018$) and the sfGFP volume was significantly reduced between 2 and 22 weeks of miBrain assembly ($p < 0.0001$, **Fig. 1f**). Consistent with α-Syn-induced neuronal death we observed a significant reduction in the volume of TUJ1 staining at 2 weeks ($p = 0.002$) and 24 weeks ($p = 0.011$) in A53T miBrains when compared to WT (**Fig. 1g**). By 24 weeks, A53T miBrains had significantly increased percentages of the sfGFP volume overlapping with pS129 Syn ($p = 0.0095$), and aggregated α-Syn ($p = 0.0381$) in comparison with 2 weeks miBrains (**Fig. 1h**), consistent with aggregation of α-Syn over time. Collectively, these results show that the miBrain can effectively model critical aspects of α-Syn pathology.

APOE4 **increases the phosphorylation and aggregation of** α**-Syn in the miBrain**

146 *APOE4* is a genetic risk factor for α-Syn in LBD[14] and AD[52,53], and it is associated with increased disease
147 severity in human studies, animal models[54,55] , and *in vitro* systems[56]. To model and investigate the
148 mechanisms by which *APOE4* promotes α-Syn pathology, we utilized isogenic iPSC lines obtained from an
149 *APOE3/3* individual CRISPR-edited to *APOE4/4*[57,58]. Monocultures of *APOE4/4* A53T neurons showed
150 similar levels of p-Syn as isogenic *APOE3/3* SNCA-A53T neurons with or without PFF exposure (**Extended**
151 **Data Fig. 2a**). Therefore, we differentiated the isogenic iPSCs into astrocytes, OPCs, endothelial cells, and
152 mural cells observing similar cell type-specific marker expression between the *APOE3/3* and *APOE4/4*
153 genotypes for each cell type (**Extended Data Fig. 2b-c**). We next generated isogenic *APOE3/3* and
154 *APOE4/4* miBrains containing SNCA-A53T neurons. Consistent with clinical studies, *APOE4/4* miBrains with
155 SNCA-A53T neurons showed significantly increased neuronal p-Syn compared to isogenic control *APOE3/3*
156 miBrains ($p = 0.0074$, **Fig. 2a**). The volume of p-Syn outside the sfGFP mask was also significantly increased
157 in *APOE4/4* miBrains compared to *APOE3/3* ($p = 0.0156$, **Extended Data Fig. 2d**), indicating that
158 endogenous non-A53T α-Syn is also phosphorylated in the *APOE4/4* miBrains. To assess whether increased
159 phosphorylation of α-Syn in the *APOE4/4* miBrain is a direct cell-autonomous effect of *APOE4/4* neurons,
160 we generated miBrains that were all *APOE4/4* except for *APOE3/3* SNCA-A53T neurons. Strikingly, we
161 observed a significant increase in p-Syn even when *APOE3/3* SNCA-A53T neurons were placed in an
162 otherwise *APOE4/4* miBrain ($p = 0.0001$, **Extended Data Fig. 2e**).

163

164 ***APOE4/4 astrocytes are responsible for increased α-Syn pathological phenotypes in human brain***
165 ***tissue****.*

166 Our results suggest that non-neuronal cell types are responsible for increased p-Syn in the *APOE4/4*
167 miBrains. To identify which *APOE4* cell types promote α-Syn pathology, we generated permutations of the
168 *APOE3/3* miBrains where each cell type was replaced with isogenic *APOE4/4* cells (**Fig 2b**). Consistent with
169 previous results, all *APOE4/4* miBrain had significantly increased p-Syn staining compared to isogenic
170 *APOE3/3* miBrains. Replacing *APOE3/3* neurons, endothelial cells, mural cells, or OPCs with their *APOE4/4*
171 isogenic counterpart did not significantly increase p-Syn immunoreactivity in the miBrain ($p = 0.99$, **Fig. 2b**).
172 However, selectively replacing *APOE3/3* astrocytes with isogenic *APOE4/4* astrocytes led to a significant
173 increase in p-Syn immunoreactivity ($p = 0.014$) reaching levels similar to the all *APOE4/4* miBrains (**Fig. 2b**),
174 suggesting that *APOE4/4* astrocytes are responsible for increasing α-Syn pathology in *APOE4* miBrain.
175 Since microglia are implicated in the clearance of α-Syn[59,60], we investigated the effect of the presence or
176 absence of microglia in the isogenic miBrains. The presence of microglia in the *APOE3/3* and *APOE4/4*
177 miBrains did not significantly alter α-Syn phosphorylation (**Extended Data Fig. 2f**). Astrocytes are
178 responsible for uptake and degradation of α-Syn released by neurons[61-63]. We found that $GFAP^+$ *APOE4/4*
179 astrocytes in the *APOE4/4* miBrain have a significantly reduced overlap with SNCA-A53T-sfGFP ($p = 0.0348$)
180 and adopt an amoeboid-like morphology with increased circularity ($p = 0.0398$) and GFAP expression ($p =$
181 0.0100) compared with *APOE3/3* miBrain astrocytes (**Fig. 2c and Extended Data Videos 2 and 3**),
182 suggesting changes in astrocytic uptake of α-Syn associated with increased reactivity. Collectively, these
183 results highlight a critical role for *APOE4/4* astrocytes in the phosphorylation and aggregation of neuronal α-
184 Syn.

185

186 ***APOE4 astrocytes have impaired processing of exogenous α-Syn.***

To investigate the mechanisms by which *APOE4* astrocytes increase the phosphorylation and aggregation of neuronal α-Syn, we first examined whether altered expression of *SNCA* in astrocytes contributes to increased abundance and phosphorylation of α-Syn in the *APOE4/4* miBrain and human brain tissue. Analysis of single-nucleus post-mortem transcriptomics data[64] revealed that *SNCA* mRNA expression is significantly ($p = 0.019$) down-regulated in astrocytes from *APOE4* carriers ($n = 10$) compared to age-matched *APOE3/3* individuals ($n = 8$) (**Fig. 3a**). We observed a similar decrease in *SNCA* mRNA expression in *APOE3/3* and *APOE4/4* iPSC-derived astrocytes[57] ($p = 0.017$) (**Extended Data Fig. 3a**) suggesting that transcriptional upregulation of *SNCA* in astrocytes is likely not responsible for increased phosphorylation and aggregation of α-Syn in the *APOE4* human brain tissue. However, immunoblotting astrocyte monocultures for α-Syn revealed that *APOE4/4* astrocytes have more total and phosphorylated α-Syn protein compared to isogenic *APOE3/3* astrocytes from two different individuals (**Fig. 3b; Extended Data Fig. 3b**) suggesting that post-translational mechanisms underlie increased α-Syn abundance in *APOE4/4* astrocytes.

Astrocytes have a well-described protective and homeostatic function of taking up and degrading neuronal α-Syn[61-63]. Given this role and our findings that *APOE4/4* astrocytes increase neuronal α-Syn phosphorylation and co-localize less with SNCA-A53T-sfGFP in the miBrain (**Fig. 2c**), we hypothesized that *APOE4/4* astrocytes have impaired processing of exogenous α-Syn. To investigate this, we incubated isogenic *APOE3/3* and *APOE4/4* astrocytes with fluorescently labeled α-Syn monomers (αSyn-HiLyte) for 24 hours. *APOE3/3* astrocytes showed a robust ability to take up αSyn within 4.5 hours ($p = 0.001$) and 6 hours ($p < 0.0001$) (**Figure 3c**). In contrast, α-Syn monomer uptake by *APOE4/4* astrocytes was significantly impaired. At 4.5 hours *APOE4/4* astrocytes had no significant ($p > 0.99$) intracellular α-Syn-HiLyte signal, but it began to increase by 6 hours ($p = 0.005$) (**Fig. 3c**). Despite delayed kinetics, at 24 hours *APOE4/4* astrocytes reached similar uptake levels as *APOE3/3* astrocytes. We then removed the media containing α-Syn and assessed the degradation of intracellular α-Syn-HiLyte over the following 24h. *APOE3/3* astrocytes had a significant decrease ($p < 0.0001$) in the α-Syn-HiLyte signal. In contrast, the signal in *APOE4/4* did not significantly decrease ($p = 0.98$) (**Fig. 3c**) suggesting that *APOE4/4* astrocytes have impaired degradation of α-Syn.

APOE4 astrocytes have impaired lysosomal function and release pathogenic α-Syn.

Since the two main systems for the degradation of intracellular proteins are the lysosomal and proteasomal pathways[65], we asked whether α-Syn was cleared via lysosomal or proteasomal degradation in astrocytes. We treated astrocytes with bafilomycinA1, a lysosomal inhibitor, or with MG-132, a proteasomal inhibitor. Lysosomal inhibition blocked the degradation of α-Syn-HiLyte ($p = 0.02$), unlike proteasomal inhibition, which had no significant effect ($p = 0.07$) on the degradation of α-Syn-HiLyte signal (**Extended Data Fig. 3c**). This confirms previous reports that α-Syn is primarily degraded through the endolysosomal pathway in astrocytes and demonstrates that *APOE4*-driven lysosomal dysfunction leads to α-Syn accumulation.

We hypothesized that the endolysosomal pathway of *APOE4/4* astrocytes is impaired in comparison to *APOE3/3* astrocytes. To assess lysosomal function, we measured the lysosome-specific proteolytic cleavage of DQ-BSA and found *APOE4/4* astrocytes have significantly decreased lysosomal proteolytic activity compared to isogenic control *APOE3/3* astrocytes in two isogenic donor lines ($p= 0.003$ and $p < 0.0001$, **Fig. 3d**). Consistent with this, immunoreactivity against the lysosomal-associated protein LAMP1 was significantly reduced in *APOE4/4* astrocytes compared to isogenic *APOE3/3* astrocytes ($p = 0.0002$ and $p = 0.0001$, **Extended Data Fig. 3d**). Likewise, staining with LysoSensor Green, a lysosomal dye that fluoresces most brightly at an acidic lysosomal pH of ~5.2, revealed that *APOE4/4* astrocytes have significantly decreased

LysoSensor Green signal, indicating decreased lysosomal acidity compared to *APOE3/3* across isogenic *APOE3/3* and *APOE4/4 astrocytes* generated from 3 different individuals ($p < 0.0001$, $p = 0.002$, $p = 0.0002$, **Extended Data Fig. 3e**). These results suggest *APOE4/4* astrocytes have decreased LAMP1 positive lysosomes with decreased lysosomal acidity, contributing to impaired lysosomal proteolytic function.

Since phosphorylated α-Syn is used as a measurement of α-Syn pathology, we next determined whether astrocytes can phosphorylate neuronal α-Syn. Therefore, we exposed *APOE3/3* and *APOE4/4* astrocytes to fresh media or conditioned media from *SNCA*-A53T neurons. At baseline, *APOE4/4* astrocytes have more endogenous p-Syn compared to *APOE3/3* astrocytes (**Fig. 3e;** $p < 0.0001$). *APOE4/4* astrocytes incubated with media previously exposed to *SNCA*-A53T neurons for 3 days, showed a further increase in p-Syn ($p = 0.007$) while *APOE3/3* astrocytes were unaffected, ($p = 0.232$) (**Fig. 3e**) indicating that *APOE4/4* astrocytes can increase α-Syn phosphorylation. However, in the miBrain and post-mortem human brain, inclusions of α-Syn are primarily found inside neurons. We found that cell culture media collected from *SNCA*-A53T neurons and then inoculated onto fresh *SNCA*-A53T neuronal cultures itself does not increase phosphorylation of neuronal α-Syn (**Fig. 3f**), suggesting that non-cell-autonomous mechanisms likely modify α-synuclein's pathogenicity. Therefore, we hypothesized that *APOE4/4* astrocytes fail to degrade α-Syn due to impaired endolysosomal function. Instead, *APOE4/4* astrocytes phosphorylate α-Syn and release the more pathogenic forms of a-Syn into the extracellular space allowing them to be taken up by neurons and promote the formation of neuronal α-Syn inclusions. To test this hypothesis, we first exposed *SNCA*-A53T neurons to conditioned media from only *APOE3/3* or *APOE4/4* astrocytes. Astrocyte-conditioned media itself did not induce significant p-Syn in *SNCA-A53T* neurons, and no significant difference was observed between *APOE3/3* and *APOE4/4* conditioned media (**Extended Data Fig. 3f**). We reasoned the low levels of α-Syn produced by astrocytes alone is not sufficient to induce phosphorylation and aggregation of neuronal α-Syn. Therefore, we performed a double conditioned media experiment where conditioned media was first collected from *SNCA*-A53T neurons and subsequently cultured with either *APOE3/3* or *APOE4/4* astrocytes. This double-conditioned media was then collected and inoculated onto fresh *SNCA*-A53T- neuron monocultures (**Fig 3f**). Neurons grown in *APOE3/3* double-conditioned media did not show a significant increase in α-Syn phosphorylation ($p = 0.601$). In contrast, *APOE4/4* double-conditioned media led to a 2.371-fold increase (± 0.315; SEM) in α-Syn phosphorylation ($p = 0.0016$). To assess whether the induction of p-Syn by *APOE4/4* double-conditioned media was a failure of astrocytes to degrade α-Syn or a modification of α-Syn, we analyzed the α-Syn species in the double-conditioned media via dot blot. Although the total levels of α-Syn in the media were not different between *APOE3/3* and *APOE4/4* astrocytes ($p = 0.894$), p-Syn and aggregated α-Syn were both significantly increased ($p < 0.0001$ and $p = 0.0051$) in media conditioned by *APOE4/4* astrocytes compared to *APOE3/3* astrocytes (**Extended Data Fig. 3g**). *APOE3/3* astrocyte double-conditioned media appeared not to change having similar p-Syn and aggregated α-Syn levels to the original *SNCA*-A53T media that was not conditioned by astrocytes ($p = 0.951$ and $p = 0.894$; **Extended Data Fig. 3g**). Collectively, these results suggest that *APOE4/4* astrocytes fail to degrade neuronal a-Syn, instead increase its phosphorylation and aggregation, and secrete these more pathological forms of α-Syn which are taken up by neurons and promote the formation of a-Syn inclusions.

Cholesterol accumulation in APOE4 astrocytes leads to dysfunctional α-Syn processing and neuronal pathology.

We next investigated how APOE4 in astrocytes leads to lysosomal dysfunction and the spread of αSyn pathogenic forms. APOE is primarily expressed in astrocytes in the brain,[66] shuttling cholesterol to neurons to maintain membranes and synapses[67,68]. APOE4 displays lower lipid transport affinity and binding

capacity[69], associated with cholesterol accumulation in astrocytic lysosomes and impaired lysosomal function[58,70]. Consistent with previous reports, transcriptomic analysis showed that genes in pathways associated with lipid storage and transport are differentially expressed compared to isogenic APOE3/3 astrocytes (**Extended Data Fig. 4a**)[58], as well as response to lipopolysaccharide and oxidative stress, which have been associated with a neurotoxic reactive phenotype[71,72]. Consistent with a dysfunctional lipid metabolism, we found that *APOE4/4* astrocytes have a significant increase in the accumulation of BODIPY-cholesterol compared to isogenic *APOE3/3* astrocytes generated from two different individuals ($p = 0.001$ and $p = 0.002$, **Fig. 4a**).

Given our findings that *APOE4/4* astrocytes have increased cholesterol and impaired endolysosomal function, resulting in increased pathogenic α-Syn secretion, we hypothesized that intracellular accumulation of cholesterol leads to impaired degradation of α-Syn by astrocytes. To test this hypothesis, we treated *APOE4/4* astrocytes with various compounds to reduce cholesterol bioavailability, either by sequestering cholesterol (2-hydroxypropyl-β-cyclodextrin (2HβCD) and methyl-β-cyclodextrin (MβCD), inhibiting cholesterol biosynthesis (atorvastatin), or promoting cholesterol efflux (efavirenz, LXR-623, and T0901317). BODIPY staining confirmed a decrease in lipid droplets, which include cholesterol, in *APOE4/4* astrocytes following treatment with 2HβCD ($p = 0.0013$) and MβCD ($p = 0.0063$), to levels comparable to *APOE3/3* astrocytes (**Fig. 4b**). 2HβCD and MβCD significantly increased *APOE4/4* lysosomal proteolytic activity, as measured by the BSA-DQ assay, compared to vehicle treated *APOE4/4* astrocytes (2HβCD: $p = 0.0005$; MβCD: $p = 0.046$) (**Fig. 4c**). However, treatment with the other compounds had no effect, or a negative effect, on *APOE4/4* lysosomal proteolytic activity. We confirmed that MβCD increases lysosomal proteolytic activity in *APOE4/4* astrocytes generated from a second individual ($p = 0.0093$), although the effect of 2HβCD was not significant ($p = 0.357$; **Extended Data Fig 4b**). These findings suggest that improvement of proteolytic function may be selective to cyclodextrin treatments.

We further evaluated the effect of 2HβCD and MβCD on lysosomes by staining treated astrocytes with the live-cell endolysosomal dye, LysoTracker. *APOE4/4* astrocytes treated with MβCD had an increase in lysosomal staining intensity compared to control *APOE4/4* astrocytes ($p = 0.044$) (**Fig. 4d**). However, 2HβCD treatment did not have a significant effect on endolysosome intensity ($p = 0.51$). In astrocytes differentiated from a second individual, both cyclodextrin treatments significantly increased endolysosomal staining intensity in *APOE4/4* astrocytes (2HβCD: $p < 0.0001$; MβCD: $p < 0.0001$) to levels comparable to *APOE3/3* astrocytes (**Extended Data Fig. 4c**). These findings suggest that lowering cholesterol burden in *APOE4/4* astrocytes with 2HβCD or MβCD treatment is sufficient to increase lysosomal and proteolytic function in *APOE4/4* astrocytes.

To evaluate the effect of 2HβCD and MβCD treatment on α-Syn uptake and degradation, we measured α-Syn-HiLyte uptake after 24 hours in astrocytes. The intensity of intracellular α-Syn-HiLyte after 24 hours significantly increased in 2HβCD and MβCD treated *APOE4/4* astrocytes (2HβCD: $p = 0.002$; MβCD: $p = 0.0003$) compared to vehicle-treated *APOE4/4* astrocytes (**Fig 4e**). This effect was replicated in isogenic astrocytes from a second individual (2HβCD: $p = 0.0004$; MβCD: $p = 0.0003$) (**Extended Data Fig 4d**). To validate that the α-Syn was being endocytosed into the endolysosomal pathway, we incubated astrocytes with α-Syn-HiLyte for 4 hours and co-stained with LysoTracker. In agreement with our other findings that *APOE4/4* astrocytes have impaired α-Syn uptake, the percentage of α-Syn-HiLyte that co-localized with LysoTracker decreased in *APOE4/4* astrocytes compared to *APOE3/3* astrocytes ($p = 0.0395$; **Extended Data Fig 4e**). However, *APOE4/4* astrocytes treated with MβCD showed increased colocalization of α-Syn-HiLyte with LysoTracker compared to vehicle-treated *APOE4/4* astrocytes ($p = 0.0343$). Strikingly APOE4/4 astrocytes treated with MβCD had similar α-Syn lysosomal localization as vehicle-treated *APOE3/*3 astrocytes ($p = 0.946$; **Extended Data Fig 4e**). Taken together, these results suggest that pharmacologically

319 reducing intracellular cholesterol in *APOE4/4* astrocytes increase α-Syn uptake and degradation potentially
320 reducing the accumulation of neurotoxic forms of α-Syn.

321 Our findings implicate astrocytes as a critical cell type in α-Syn processing in the genetic context of *APOE4.*
322 However, α-Syn pathology in Lewy body diseases is characterized by inclusions found within neuronal
323 projections and soma. To investigate whether improved lysosomal activity in cyclodextrin-treated astrocytes
324 affected neuronal α-Syn phosphorylation, we returned to the miBrain model. After 7 days of treatment with
325 MβCD, the levels of neuronal phosphorylated α-Syn were significantly reduced in MβCD treated *APOE4/4*
326 miBrains ($p = 0.031$) when compared to untreated *APOE4/4* miBrains and restored phosphorylation to levels
327 that were not statistically different from *APOE3/3* miBrains ($p = 0.099$) (**Fig. 4f**). These results show that
328 MβCD treatment reduces α-Syn phosphorylation in neurons likely via restoration of lysosomal activity and α-
329 Syn processing in astrocytes, alleviating cells of the cytotoxic burden of α-Syn aggregation. This may open
330 a therapeutic avenue for cholesterol-lowering pharmacological interventions in the treatment of
331 synucleinopathies and AD with Lewy Bodies, particularly in *APOE4* carriers.

332

333 **Discussion:**

334 By combining stem cell and genetic engineering, we extended our recently developed miBrain system[27] to
335 model α-Synuclein pathological phenotypes and dissect disease-relevant cellular and molecular
336 mechanisms in human brain tissue in a dish. miBrains containing neurons, glia, and vascular cells displayed
337 trackable α-Syn pathological forms in neurons and neuronal death as early as 2 weeks and as late as 6
338 months in culture. Cryopreservation of pre-assembled tissue allowed better reproducibility and decreased
339 variability of our methods, enabling complex multivariate experiments. Using a genetic mix-and-match
340 permutation approach that is unique to miBrains, we found that *APOE4* promotes neuronal α-Syn
341 accumulation specifically via astrocytes. *APOE4*-induced cholesterol accumulation causes endolysosomal
342 dysfunction and impaired α-Syn processing in astrocytes. This leads to the astrocytic secretion of pathogenic
343 α-Syn that seeds α-Syn aggregation and phosphorylation on neurons. We found that pharmacologically
344 increasing cholesterol efflux restored astrocytic endolysosomal function and prevented the accumulation of
345 neuronal p-Syn in human brain tissue. These results establish a causal link between cholesterol
346 dysregulation and α-Syn pathology in *APOE4* carriers, which may influence the progression of classical
347 synucleinopathies and AD with Lewy Bodies.

348 Cholesterol dysregulation in *APOE4* astrocytes has been related to a reduced expression of lipid transport
349 genes[57], reduced cholesterol efflux[58], and increased accumulation of cholesterol in lysosomes[70]. This was
350 associated with increased secretion of inflammatory cytokines and reduced amyloid-β processing[73].
351 Genetically induced cholesterol accumulation has been shown to promote an increased secretion of
352 exosomes[74]. Cholesterol accumulation might convert astrocytes into a secretory phenotype, including
353 releasing pathogenic α-Syn and other cargo. While it is known that neurons can secrete pathogenic α-Syn[75]
354 that is taken and processed by astrocytes[61-63], to our knowledge, the release of pathogenic α-Syn by
355 dysfunctional astrocytes has not been previously described.

356 Our results suggest that *APOE4* leads to a disease-relevant astrocytic phenotype characterized by
357 endolysosomal dysfunction driven by cholesterol accumulation, leading to suboptimal processing and
358 secretion of pathogenic α-Syn that is further taken by neurons, exacerbating Lewy-like pathology. We found
359 pharmacological cholesterol reduction using methyl-β-cyclodextrin prevented α-Syn accumulation in *APOE4*
360 human brain tissue. Clinical trials on cyclodextrins have primarily focused on NPC1 disease, with a recent

361 Phase I/II trial describing improved clinical symptoms and mild-to-moderate adverse effects after intravenous
362 administration of hydroxypropyl-β-cyclodextrin[76]. Other cholesterol-lowering drugs such as statins remain the
363 primary approach to reduce cholesterol in patients without NPC1. In a mouse model of α-Syn pathology,
364 feeding a high-fat diet increased α-Syn aggregation and that was reduced by treatment with brain-penetrating
365 statins, suggesting that statins can lower α-Syn aggregation by reducing brain cholesterol[77]. A meta-analysis
366 study reported that statins can reduce the risk of Parkinsonism in older adults and that this effect is mediated
367 by reduced atherosclerosis[78], but a randomized clinical trial evaluating the benefit of the most used type of
368 statin, simvastatin, found no evidence to support its use as a disease-modifying therapy in Parkinson's
369 disease[79]. We discovered that *APOE4* increases α-Syn pathology via cholesterol dysregulation, suggesting
370 that the *APOE* genotype may impact whether cholesterol-lowering medications can benefit classic
371 synucleinopathies and co-pathological presentations of pathogenic α-Syn such as AD with Lewy Bodies.

372 We present a novel, scalable stem cell-based tissue platform capable of modeling human neurodegenerative
373 phenotypes in a dish. Collectively, our findings establish a mechanistic link between cholesterol accumulation
374 and α-Syn pathology mediated by *APOE4* astrocytes and offer therapeutic opportunities for *APOE4* carriers
375 with α-Syn pathology in classical synucleinopathies like LBD, as well as in AD with Lewy Bodies and other
376 neurodegenerative conditions. Future optimization of the miBrain system to enable microvascular perfusion
377 and support extended experimentation and drug testing will further enhance its utility, paving the way for
378 deeper exploration of neurodegenerative mechanisms and therapeutic testing.

379 **Acknowledgments**

380 We would like to thank Tatyana Kareva for technical support and all members of the Blanchard Lab for
381 scientific discussions. We would like to thank Elena Coccia for revising the manuscript. We acknowledge the
382 use of BioRender for generation of illustrative cartoons.

383 This work has been funded in part with federal funds from NASA under contract #80ARC022CA004 titled
384 "Identification of Biomarkers and Pathological Mechanisms via Longitudinal Analysis of Neurological and
385 Cerebrovascular Responses to Neurotoxic Stress Using a Multi-cellular Integrated Model of the Human
386 Brain." This research was funded in whole or in part by Aligning Science Across Parkinson's (ASAP-00458)
387 through the Michael J. Fox Foundation for Parkinson's Research (MJFF). For open access, the authors have
388 applied a CC-BY public copyright license to all Author Accepted Manuscripts arising from this submission.
389 This work was also supported by funding from the NIH/NINDS (R01NS114239 and UH3NS115064), and the
390 CureAlz Fund. C.G. was supported by funding from the NIH/NIA (T32AG04968) and NIH/NINDS
391 (F31NS13090).

392 **Author Contributions**

393 Conceptualization: L.A.M.L, C.G., and J.W.B.; Methodology: L.A.M.L., C.G., J.W.B., A.N., and V.K.;
394 Investigation: L.A.M.L., C.G., A.B., R.B.R., B.R.S., and A.U.; Writing – Original Draft: L.A.M.L and C.G.;
395 Writing – Review & Editing: L.A.M.L., C.G., J.W.B., A.N., and V.K; Supervision: J.W.B.; Funding Acquisition:
396 J.W.B.

397 **Declaration of Interests**

398 V.K. is a cofounder of and senior advisor to DaCapo Brainscience and Yumanity Therapeutics, companies
399 focused on CNS diseases. L.A.M.L, J.W.B., C.G., and R.B.R. are inventors on patent applications filed by
400 Mount Sinai Innovation Partners on the methods described in this study. A.N. and V.K. are inventors on a
401 patent application filed by Brigham and Women's Hospital related to the induced inclusion iPSC models.

402 **Methods:**

403 Key Resources Table

REAGENT OR RESOURCE	SOURCE	IDENTIFIER
Chemicals, peptides, and recombinant proteins		
2-hydroxypropyl-β-cyclodextrin	Sigma	Cat# C0926
Accutase	Stemcell	Cat# 07920
Activin A	Peprotech	Cat# 120-14P
Astrocyte Growth Supplement	ScienCell	Cat#1852
Astrocyte Medium (AM)	ScienCell	Cat# 1801
a-Synuclein (1-140) HiLyte Fluor 488	Anaspec	Cat# AS-55457
Atorvastatin	Sigma	Cat# SML3030
B27	Gibco	Cat# 17504044
B27 without Vitamin A	Gibco	Cat# 12587010
Bafilomycin A1	Millipore	Cat# B1793
BDNF	Peprotech	Cat# 450-02
Biotin	Sigma	Cat#B4639
Blasticidin	Gibco	Cat # A1113903
BMP4	Peprotech	Cat# 120-05ET
BODIPY-Cholesterol	Cayman	Cat# 24618
CD Lipids	Gibco	Cat# 11905031
CHIR99021	Tocris	Cat# 4423
CNTF	Peprotech	Cat# 450-13
DAPT	Cayman	Cat# 13197
Dibutyryl cAMP	Biogems	Cat# 1698950
DMEM	Gibco	Cat# 11965092
DMEM/F12 with GlutaMAX	Gibco	Cat# 10565018
Doxycyline	Millipore	Cat# D3072
DQ-BSA Red	Thermo Scientific	Cat # D12051
DRAQ5	Thermo Scientific	Cat# 52251
Efavirenz	MedChem Express	Cat# HY10572
FGF-basic	Peprotech	Cat# 100-18B
Forkskolin	R&D	Cat# 1099/10
GDNF	Peprotech	Cat# 450-10
Gelxtrex	Gibco	Cat# A1413201
GlutaMAX	Gibco	Cat# 35050061
HGF	Peprotech	Cat# 100-39H
Hoechst33342	Thermo Scientific	Cat# 62249
Human Endothelial SFM	Gibco	Cat# 11111044
IGF-1	Peprotech	Cat# 100-11
Insulin	Sigma	Cat# I9278
Laminin	Gibco	Cat# 23017015

L-Ascorbic Acid	Fisher Scientific	Cat# BP351
LipidSpot	Biotium	Cat# 70069-T
LDN193189	Tocris	Cat# 6053
Lipofectamine Stem Transfection Reagent	Invitrogen	Cat# STEM00001
LXR-623	MedChem Express	Cat# HY-10629
LysoSensor Green DND-189	Thermo Scientific	Cat# L7535
LysoTracker DeepRed	Thermo Scientific	Cat# L12492
MEM-Non-Essential Amino Acids	Gibco	Cat#111400050
Methyl-β-cyclodextrin	Cayman	Cat #21633
N2	Gibco	Cat# 17502048
Neurobasal	Gibco	Cat# 21103049
NT3	Peprotech	Cat# 450-03
PDGF-AA	Peprotech	Cat# 100-13A
PDGF-BB	Peprotech	Cat# AF-100-14B
Penicillin-Streptomycin	Gibco	Cat# 15140122
Puromycin	Gibco	Cat# A1113803
Retinoic Acid	MIllipore	Cat# R2625
SAG	Cayman	Cat# 11914
SB431542	Stemgent	Cat# 04-0010
StemFlex	Gibco	Cat# A3349401
T0901317	MedChem Express	Cat# HY-10626
TrypLE Select	Gibco	Cat# 12563011
VEGF-A	Peprotech	Cat#100-20
Y-27632	Tocris	Cat# 1254
Antibody		
a-Synuclein (MJFR1)	Abcam	Cat# ab138501
a-Synuclein (phospoho S129) (MJF-R13)	Abcam	Cat# ab168381
a-Synuclein pS129 (D1R1R)	CellSignaling	Cat# 23706
a-Synuclein pS129 (EP1536Y)	Abcam	Cat# ab51253
aSynuclein aggregate (MJFR-14-6-4-2)	Abcam	Cat# ab209538
AQP4	Invitrogen	Cat# PA5-53234
CD31/PECAM-1	R&D Systems	Cat# AF806
CD49f	BioLegend	Cat# 313602
GFAP	Invitrogen	Cat# 14-9892-82
IBA1	NovusBio	Cat# NB100-1028
LAMP1	NovusBio	Cat# NBP2-25183
MAP2	Biolegend	Cat# 822501
MBP	EMD Millipore	Cat# AB9348
MRF	EMD Millipore	Cat# ABN45
Neurofilament-H	BioLegend	Cat# 822601
NG2	EMD Millipore	Cat# Ab5320
S100β	Sigma-Aldrich	Cat# 2532

Tom20 (F-10)	Santa Cruz Biotechnologies	Cat# sc-17764
Tubulin β 3 (TUBB3) (TUJ1)	BioLegend	Cat# 801202
VECAD	R&D Systems	Cat# AF938
β-Actin	Invitrogen	Cat# am4302
Critical commercial assays		
Criterion 4-15% TGX precast gel	BioRad	Cat# 5671084
LDH-Glo Cytotoxicity Assay	Promega	Cat# J2381
Pierce BCA Protein Assay	Thermo Scientific	Cat# 23223
Experimental models: Cell lines		
A53T-1A CORR28	Harvard Medical School	RRID: CVCL_E3CE
AG09173 iPSCs	Massachusetts Institute of Technology	RRID: CVCL_4L66
ADRC5 iPSCs	UCI	
KOLF2.1J iPSCs	Jackson Laboratories	RRID:CVCL_B5P3
Recombinant DNA		
piggyBac-rtTA (4th_Gen)-NGN2-2A-PURO-IRES-SNAP	Addgene	Cat# 209077
piggyBac-rtTA (4th_Gen)-SNCA(A53T)-sfGFP-IRES-NGN2-puro	Addgene	Cat# 209080
piggyBac-rtTA (4th_Gen)-SNCA(A53T-DNAC)-sfGFP-IRES-NGN2-puro	Addgene	Cat# 209081
PB_iETV2_P2A_GFP_Puro	Addgene	Cat# 168805
Software and algorithms		
Fiji	Schindelin, J. et al., 2012	imagej.net/ software/fiji/
Nikon NIS Elements software	Nikon	microscope.healthcare.nikon.com
GraphPad Prism	GraphPad Software	graphpad.com
Other		
48-well plate	P48G-1.5-6-F	MatTek
96-well plate with cover glass thickness polystyrene bottom	Greiner Bio-One	655096
Ti2E Ax R Confocal Microscope	Nikon	microscope.healthcare.nikon.com

Resource availability

Lead Contact

Further information and requests for resources and reagents should be directed to and will be fulfilled by the lead contact, Dr. Joel W. Blanchard (joel.blanchard@mssm.edu).

Material availability

This study did not generate new unique reagents

411 **Data and code availability**

412 • All raw data will be made available on Mendeley upon paper acceptance and will be made publicly
413 available.
414 • Original code relating to scRNAseq pseudobulk analysis will be made available on Mendeley upon
415 paper acceptance and will be publicly available.
416 • Any additional information required to reanalyze the data reported in this paper is available from the
417 lead contact upon request.

418 **Human iPSC cultures**

419 All human iPSCs were maintained in feeder-free conditions in StemFlex™ medium (Gibco) on Geltrex™
420 Matrix (Thermo Fisher Scientific) pre-coated plates. All iPSC lines used in this study are listed in the Key
421 Resource Table. CRISPR/Cas9 genome editing was performed as previously described[57]. Human iPSCs
422 were grown as colonies in StemFlex™ medium until they reached 60-70% confluency. At this point, iPSCs
423 were either passaged for maintenance using 0.5 mM EDTA to gently lift colonies or harvested using
424 Accutase™ cell detachment solution for 5-10 minutes at 37C to start a differentiation protocol as singularized
425 cells.

426 **Differentiation of human iPSCs into neurons**

427 Neuron differentiation was adapted from Zhang *et al*.[30] and Lam *et al*.[29]. Briefly, iPSCs were transfected with
428 PiggyBac plasmids to confer doxycycline-inducible expression of the Neurogenin- 2 gene (*NGN2*, Addgene
429 Plasmid #209077) alone or combination with SNCA-A53T-sfGFP (Addgene Plasmid: 209080) or A53T-
430 DNAC-SNCA-sfGFP (Addgene Plasmid: 209081), using Lipofectamine™ Stem Transfection Reagent.
431 Briefly, dissociated iPSCs were plated at ~104,000 cells/cm^2 onto Geltrex™-coated plates, in StemFlex™
432 supplemented with 10 μM Y27632 and 5 μg/mL doxycycline (day 0). At day 1, medium was replaced with
433 Neurobasal N2B27 medium (Neurobasal, 1x B-27, 1x N-2, 1x MEM-NEAA, 1x GlutaMAX, 1% penicillin-
434 streptomycin) supplemented with 10uM SB431542, 100 nM LDN, 5 μg/mL doxycycline, 5 μg/mL Blasticidin.
435 On day 2, the medium was replaced with Neurobasal N2B27 media supplemented with 10uM SB431542,
436 100 nM LDN, 5 μg/mL doxycycline, 1 μg/mL puromycin. On days 3-6, the medium was replaced daily with
437 Neurobasal N2B27 media supplemented with 5 μg/mL doxycycline, and 1 μg/mL puromycin. At day 7, cells
438 were dissociated with Accutase and either seeded into miBrains (see bellow) or seeded into 2D monocultures
439 on Poly-L-Ornithine and Laminin pre-coated plates at 156,250 cells/cm^2, in Neurobasal N2B27 with 5 μg/mL
440 doxycycline and 10 μM Y27632. For 2D cultures, on day 8, wells were gently topped with Neurobasal N2B27
441 supplemented 20ng/mL BDNF, 20ng/mL GDNF, 1mM dcAMP, 2ug/mL Laminin, and 1 uM AraC, using the
442 same volume of medium in the wells. At day 11, media is replaced with Neurobasal N2B27
443 supplemented with 10ng/mL BDNF, 10ng/mL GDNF, 0.5 mM dcAMP, 1ug/mL Laminin. This medium was
444 used for half-media changes every 3-4 days.

445 **Differentiation of human iPSCs into astrocytes**

446 Astrocytes were generated using previously published protocols for iPSC-derived NPC (Chambers *et al*.)[31]
447 and astrocyte (TCW *et al*.)[32] differentiation. Briefly, dissociated iPSCs were plated at 100,000 cells/cm^2 onto
448 Geltrex™-coated plates, in pre-warmed StemFlex™ supplemented with 10 μM Y27632. Cells were fed every
449 other day with StemFlex™ until they reached >95% confluence. Once cells reached confluence, the medium
450 was replaced with NPC medium (1:1 DMEM/F12: Neurobasal Medium, 1x N-2 Supplement, 1x B-27 Serum-
451 Free supplement, 1x GlutaMAX Supplement, 1x MEM-NEAA, 1% penicillin-streptomycin) supplemented with
452 10 μM SB43152 and 100 nM LDN193189 (day 0). From days 1 to 9, cells are fed daily with NPC medium

453 plus 10 μM SB43152 and 100 nM LDN193189. At day 10, cells were split with Accutase and replated onto
454 fresh Geltrex™-coated plates, in NPC media supplemented with 20 ng/mL bFGF and 10 μM Y27632. From
455 days 11 to 13, cells were fed with NPC media plus 20 ng/mL bFGF. At day 14, cells were split with Accutase
456 and re-seed onto fresh Geltrex™-coated plates, in NPC media plus 20 ng/mL bFGF and 10 μM Y27632.
457 Starting from day 15, cells were fed every 2-3 days with Astrocyte Medium (AM, ScienCell) and passaged
458 using Accutase once they reached 90% confluence. From this point, NPCs were fully differentiated into
459 astrocytes in 30 days. NPCs and fully differentiated astrocytes were cryopreserved in the freezing medium
460 consisting of 90% knockout serum replacement (KSR) and 10% dimethyl sulfoxide (DMSO).

461 **Differentiation of human iPSC into brain microvascular endothelial cells**

462 Brain endothelial cell differentiation was adapted from the protocols from Blanchard *et al.*, Qian *et al.,* and
463 Wang *et al*. [33,36,80]. Briefly, iPSCs were transfected with a PiggyBac plasmid to confer doxycycline-inducible
464 expression of the ETS variant transcription factor 2 (*ETV2*, Addgene Plasmid #168805), using
465 Lipofectamine™ Stem Transfection Reagent. Inducible ETV2-iPSCs were grown until 60-70% confluency,
466 dissociated with Accutase, and plated at 20,800 cells/cm^2 onto Geltrex™-coated plates in StemFlex™
467 supplemented with 10 μM Y27632 (day 0). On day 1, the medium was replaced with DeSR1 medium
468 (DMEM/F12 with GlutaMAX, 1× MEM-NEAA, 1× penicillin-streptomycin) supplemented with 10 ng/mL BMP4,
469 6 μM CHIR99021, and 5 μg/mL doxycycline. On day 3, the medium was replaced with DeSR2 medium
470 (DeSR1 media, 1x N-2, 1× B-27) supplemented with 5 μg/mL doxycycline. At days 5 and 7, the medium was
471 replaced with hECSR medium (Human Endothelial Serum-free Medium, Gibco, 1× MEM-NEAA, 1× B-27,
472 1% penicillin-streptomycin) supplemented with 50 ng/mL VEGF-A, 2 μM Forskolin, and 5 μg/mL doxycycline.
473 At day 8, cells were dissociated using Accutase and re-seed onto fresh Geltrex™-coated plates in hECSR
474 supplemented with 50 ng/mL VEGF-A and 5 μg/mL doxycycline. This medium was used for every 2-3 days
475 medium change to maintain cells for up to 1 week until ready for tissue assembly (miBrain or JAMs).

476 **Differentiation of human iPSCs into mural cells**

477 Mural cells were differentiated using previously published protocol from Patsch *et al.*[37]. Dissociated iPSCs
478 were plated at 37,000 to 40,000 cells/cm^2 onto Geltrex™-coated plates, in StemFlex™ supplemented with
479 10 μM Y27632 (day 0). On day 1, the medium was replaced with N2B27 medium (1:1 DMEM/F12:
480 Neurobasal media, 1x B-27, 1x N-2, 1x MEM-NEAA, 1x GlutaMAX, 1% penicillin-streptomycin)
481 supplemented with 25 ng/mL BMP4 and 8 μM CHIR99021. At days 3 and 4, the medium was replaced with
482 N2B27 media supplemented with 10 ng/mL Activin A and 10 ng/mL PDGF-BB. At day 5, mural cells were
483 dissociated with Accutase and re-seeded onto fresh 0.1% gelatin-coated plates at 35,000 cells/cm^2, in N2B27
484 supplemented with 10 ng/mL PDGF-BB. This medium was used every 2-3 days medium was change for
485 another 5–7 days. Cells were then banked in freezing medium (90% KSR/ 10% DMSO) and expanded in
486 N2B27 until ready for tissue assembly (miBrain or JAMs).

487 **Differentiation of human iPSCs into oligodendrocyte progenitor cells (OPCs)**

488 OPC differentiation was adapted from Douvaras et al, 2014[81]. Briefly, iPSCs were dissociated into single
489 cells using Accutase and seeded at near-confluent density. Differentiation began the next day (designated
490 as day 0) by culturing the cells in DMEM/F12 (1:1) medium supplemented with N2, 10 μM SB431542, 100
491 nM LDN 193189, and 100 nM all-trans retinoic acid (RA), with daily medium changes. On day 8, 1 μM SAG
492 was added to the differentiation medium, maintaining the presence of 10 μM SB431542 and 100 nM LDN
493 193189. By day 12, adherent cells were detached and transferred to low-attachment plates to form cell
494 spheres. These spheres were cultured in DMEM/F12 (1:1) medium containing N2, RA, and SAG. On day 30,

495 spheres were plated onto poly-L-ornithine/laminin-coated plates to allow cells to migrate outward. At this
496 stage, the medium was replaced with DMEM/F12 (1:1) supplemented with N2, B27, 10 ng/ml PDGF-AA, 10
497 ng/ml IGF, 5 ng/ml HGF, 10 ng/ml NT3, 25 µg/ml insulin, 100 ng/ml biotin, 1 µM cAMP, and 60 ng/ml T3. By
498 day 75, cells were harvested, dissociated, and purified using NG2-specific magnetic-activated cell sorting
499 (MACS). The enriched cells were expanded in DMEM/F12 (1:1) medium supplemented with N2, B27 without
500 Vitamin A, 10 ng/ml PDGF-AA, 10 ng/ml β-FGF, and 10 ng/ml NT3 until ready for tissue assembly (miBrain
501 or JAMs).

502 **Differentiation of human iPSCs into microglia**

503 iPSC-derived microglia were differentiated as previously shown[39,82] via an intermediate differentiation step
504 into hematopoietic progenitor cells (HPCs). For the generation of HPCs, the STEMdiff Hematopoietic Kit
505 (cat#: 05310; StemCell Technologies) was used, according to the manufacturer's manual. Briefly, when 70%
506 confluent (day 0), iPSCs were harvested and passaged at a density of 20-40 colonies per well in a 6-well
507 coated with 0.1mg/mL Matrigel (cat#: 354234; Corning). On day 1, Medium A was added to the culture, and
508 on day 4 it was switched to Medium B until complete HPC maturation on days 11-13. Fully differentiated
509 HPCs, floating in the medium and detached from the colonies, were collected for microglial differentiation or
510 frozen in Stem-CellBanker (cat#: 11924; AMSBIO) supplemented with microglial cytokines. For the
511 generation of mature microglia, differentiated HPCs were collected and transferred into Matrigel coated 6-
512 well plate at a confluency of 350k HPCs per well. The differentiation takes 25-28 days, during which HPCs
513 are cultured in microglia media consisting of DMEM/F12 (cat#: 11320-033; Gibco), with 2X B27 (cat#:
514 17504044; Thermo Fisher Scientific), 0.5X N2 (cat#: 17502048; Thermo Fisher Scientific), 1X Glutamax
515 (cat#: 35050061; Gibco), 1X non-essential amino acids (cat#: 11-140-050; Gibco, 400 mM Monothioglycerol
516 (cat#: M6145; Millipore Sigma), and 5 mg/mL human insulin (cat#: I9278; Millipore Sigma), freshly
517 supplemented with 100 ng/mL IL-34 (cat#: 200-34; PeproTech), 50 ng/mL TGFβ1 (cat#: 100-21; PeproTech),
518 and 25 ng/mL M-CSF (cat#: 300-25; PeproTech). Microglia were added to miBrains within the pool of Geltrex
519 encapsulated cells at the time of miBrain assembly. MiBrains were maintained in miBrain media
520 supplemented with 100 ng/mL IL-34 and 25 ng/mL M-CSF for 1 week and then switched to miBrain media
521 supplemented with 25 ng/mL M-CSF until downstream experiments.

522 **3D Tissue Assembly for miBrains, co-cultures or Cryopreservation**

523 Neurons, astrocytes, endothelial cells, mural cells, and OPCs were dissociated using Accutase or TryplE
524 Select (astrocytes). Cells were resuspended in corresponding media, counted, and resuspended at 1 x 10^6
525 cells/ mL. For miBrains, a tube was prepared to contain 5 x 10^6 neurons, 5 x 10^6 endothelial cells, 1 x 10^6
526 astrocytes, 1 x 10^6 OPCs, and 1 x 10^6 mural cells per 1 mL. Microglia was added for a subset of miBrains at
527 the ratio of 1.67 x 10^6 per 1 mL. Pooled cells were spun down at 200 x g for 5 min at RT. Media was aspirated
528 carefully, leaving the cell pellet undisturbed. The cell pellet was placed on ice and resuspended in 1 mL
529 Geltrex™ supplemented with 10 µM Y27632 and 5 µg/mL doxycycline, avoiding air bubbles and keeping it
530 on ice to prevent premature Geltrex polymerization and inability to seed miBrains properly. To generate
531 miBrain tissue that adopted a free-floating, organoid-like morphology over time, 25-50 µL of encapsulated
532 cell suspension were seeded per inner glass-bottom well of a 48-well MatTek plate (MatTek). To generate
533 miBrain tissue that remained attached to the plate (more suitable for automated imaging) while conserving
534 3D morphology, 10 µL of encapsulated cell suspension were seeded per well of a 96-well µClear plastic-
535 bottom plate (Greiner). For JAMs assembly and cryopreservation, a tube containing 5 x 10^6 endothelial cells,
536 1 x 10^6 astrocytes, 1 x 10^6 OPCs, and 1 x 10^6 mural cells per 1 mL was prepared. Pooled cells were spun
537 down at 200 x g for 5 min at RT and cryopreserved in miBrain freezing media (60% KSR, 30% hECSR
538 medium, 10% DMSO, 10 µM Y27632, 50 ng/mL VEGF-A). Upon thaw, cell viability was assessed, and the

539 appropriate volume of neurons needed to conserve the original miBrain cell-to-cell ratio was added to the
540 pooled cell suspension, which was spun again, encapsulated, and seeded as described above. After
541 miBrains were seeded, the plates were transferred into a 37 ˚C 95%/5% Air/CO2 incubator for 30 minutes to
542 allow the Geltrex™ to polymerize. After polymerization of the gel, miBrain week-1 medium (Human
543 Endothelial Serum-free Medium, 1x Pen/Strep, 1X MEM-NEAA, 1X CD Lipids, 1x Astrocyte Growth
544 Supplement (ScienCell), 1x B27 Supplement, 10ug/mL Insulin, 1μM cAMP-dibutyl, 50μg/mL Ascorbic acid,
545 10ng/mL NT3, 10ng/mL IGF, 100ng/mL Biotin, 60 ng/mL T3, 50 ng/mL VEGF, 1μM SAG, 5 μg/mL
546 doxycycline) was added to each well, ensuring complete submersion of the culture in media (250-500uL per
547 well of a 48-well matTek plate, 100 to 200 uL per well of a 96-well plate). Half media change was performed
548 every 2-3 days. On day 8 after miBrain seeding, the media was changed to miBrain week-2 medium (Human
549 Endothelial Serum-free Medium, 1x Pen/Strep, 1X MEM-NEAA, 1X CD Lipids, 1x Astrocyte Growth
550 Supplement (ScienCell), 1x B27 Supplement, 10ug/mL Insulin, 1μM cAMP-dibutyl, 50μg/mL Ascorbic acid,
551 10ng/mL NT3, 10ng/mL IGF, 100ng/mL Biotin, 60 ng/mL T3, 5 μg/mL doxycycline). Cultures were used for
552 downstream assays after 2 weeks.

553 **Exposure of tissue to exogenous α-Synuclein**

554 miBrains were exposed to 4 mg/ml of Human Recombinant Alpha Synuclein Protein Aggregates (Pre Formed
555 Fibrils, PFFs, from StressMarq, #SPR-322, or Abcam, #ab218819). PFFs were sonicated in a water bath
556 (VWR Ultrasonic Cleaner) immediately before adding to the cultures, using 10 cycles of 30 sec on, and 30
557 sec off. Free-floating miBrains incubated with Alpha-Synuclein had a media change after 48h and were fixed
558 in 4% paraformaldehyde after 2 weeks.

559 **Induction of α-Syn pathology via expression of SNCA-A53T**

560 Neurons with inducible expression of *SNCA* with the A53>T mutation (A53T), which increases α-Syn's
561 propensity to aggregate[44,45], were generated from iPSC as described above. Cells were harvested on day 7
562 of the differentiation and cultured in 2D on Poly-L-Ornithine and Laminin pre-coated plates at 156,250
563 cells/cm^2, or encapsulated for 3D cultures in Geltrex at 50,000 cells for 10 uL of Geltrex, or added to JAMs
564 for miBrain assembly as described above. The cultures were maintained for 18 days with or without PFFs.
565 For the cultures that received PFFs, 4 mg/ml PFFs were added to the media on day 4 after assembly. The
566 media was half-changed every 2-3 days. As an additional control, we generated neurons where SNCA-A53T
567 was overexpressed without the non-amyloid component (NAC) domain, which is required for α-Syn
568 aggregation.[83]

569 **Immunofluorescence**

570 2D cultures were fixed in 4% paraformaldehyde for 15 min at room temperature and rinsed with PBS. 2D
571 cultures were blocked in 0.3% Triton-X100, 5% normal donkey serum in PBS for 30 min., and then with
572 primary antibodies diluted in blocking buffer overnight at 4°C. Cultures were rinsed 3 times with 0.3% Triton-
573 X100 in PBS for 15 min each, and incubated with secondary antibodies (and Hoechst 33342) diluted at
574 1:1000 in blocking buffer for 2h at room temperature. Cultures were rinsed 3 times with PBS for 15 minutes
575 and left in PBS for image acquisition. 2D neuronal cultures were blocked in 0.1% Triton-X100, and 10%
576 normal donkey serum in PBS, antibodies were diluted in 0.02% Triton-X100 and 2% normal donkey serum
577 in PBS, and washes were done with PBS. All other conditions were kept the same as the other cell types.

578 3D cultures and miBrains were fixed in 4% paraformaldehyde overnight at 4°C and rinsed with PBS. 3D
579 cultures and miBrains were incubated in blocking solution (0.3% Triton-X100, 5% normal donkey serum, in
580 PBS) overnight at 4°C and then with primary antibodies diluted at 1:500 in blocking solution for 2-3 nights at

581 4°C. Cultures were rinsed 5 times with 0.3% Triton-X100 PBS for 30 min each and incubated with secondary
582 antibodies and Hoechst 33342 (Thermo 62249) diluted at 1:1000 in blocking solution for 2-3 nights at 4°C.
583 Cultures were rinsed 5 times with 0. 3% Triton-X100 PBS for 30 min each then rinsed and left in PBS for
584 image acquisition.

585 **Image acquisition and quantification**

586 Images were acquired using a confocal microscope (Leica Stellaris or Nikon AX R). For quantification, 10-
587 20 μm Z-stack images were acquired at 10x or 20x, 4 fields per well or free-floating miBrains. Volume
588 measurements on Z-stacks were performed using Nikon AX R built-in quantification software. Statistical
589 analyses were performed using GraphPad Prism Software. Normality and Lognormality tests D'Agostino &
590 Pearson, Anderson-Darling, Shapiro-Wilk and Kolmogorov-Smirnov were performed to determine the choice
591 for parametric or non-parametric testing. Post hoc tests on ANOVAs were conducted based on GraphPad
592 reccomendations.

593 **Human iPSC-derived astrocyte bulk RNAseq analysis**

594 Fragments Per Kilobase of transcript per Million mapped reads (FPKM) values were obtained from published
595 bulk RNA-seq data of isogenic human iPSC-derived astrocytes expressing either *APOE3/3* or *APOE4/4*[57].
596 FPKM values were log2-transformed with an offset of 0.1 and genes with zero variance across all the samples
597 were excluded. To focus on genes with meaningful variability, an additional filtering step was applied to retain
598 genes above the 10th percentile (variance > 0.033) after the removal of the zero-variance genes. Differential
599 expression analysis was performed using the limma package in R. A design matrix was constructed to model
600 the experimental conditions (APOE3 vs. APOE4) and sample-specific array weights were estimated using
601 the array Weights function with a prior.n value of 100 to help stabilize weight estimation. A linear model was
602 then fit to the log-transformed, filtered expression data using lmFit, and empirical Bayes moderation was
603 applied via the eBayes function, with trend and robust both set to TRUE. Differentially expressed genes
604 (DEGs) were defined as having an absolute log2 fold change > 0.5 and adjusted p-value (false discovery
605 weight) < 0.05. A volcano plot was then generated using the ggplot2 package and genes meeting the DEG
606 thresholds were highlighted. Enrichment analysis was performed on the upregulated and downregulated
607 DEGs separately using the clusterProfiler package. Pathways were identified through Gene Ontology (GO)
608 database. The top 10 pathways for each direction (upregulated and downregulated) were selected based on
609 adjusted p-values.

610 **Human astrocyte scRNAseq pseudobulk analysis**

611 The processed dataset was downloaded from Haney et al[64]. Unless otherwise stated, all following analyses
612 were performed in R using the package Seurat[84]. Aligning with the quality control protocol from the source
613 publication, cells with nFeature < 500, nCount < 1000, and mitochondrial and ribosomal reads > 10% were
614 discarded. Doublets were removed using the DoubletFinder package[85]. Following the standard Seurat
615 pipeline with default parameters, raw gene counts were normalized, the top 2,500 highly variable genes were
616 identified, and the data was scaled. Harmony was used to integrate the patient samples, and the top 20
617 principal components were used in Seurat's FindNeighbors, FindClusters (0.2 resolution), and RunUMAP
618 functions. Cell-type annotation was manually performed using the marker genes described in Haney et al.
619 and clusters not enriched for these marker genes were removed from further analysis. Pseudobulked
620 samples were generated by summing the raw counts for each patient sample and normalized using Seurat's
621 AggregateExpression() function.

622 **Isogenic iPSC-derived astrocyte RNAseq analysis**

623 The raw counts from iPSC-derived astrocyte bulk RNAseq were downloaded from Lin et al.[57] Raw counts
624 were processed using the DeSeq2 package[86] and normalized using the counts() function with normalized set
625 to TRUE.

626 **DQ-BSA proteolytic activity assay**

627 Astrocytes were seeded at 10,000 cells/well of a 96 well µClear plastic bottom plate (Greiner 655090) in AM.
628 The following day, media was changed to FBS-free maturation media (50% DMEM/F12, 50% Neurobasal,
629 1X B27 without Vitamin A, 1X N2, 1X NEAA, 1X GlutaMAX, 1% penicillin-streptomycin). Half of the wells
630 were treated with 100 nM BafilomycinA1 to inhibit lysosomal function as a negative control. The next day,
631 cells were pulsed with 1mM DQ-BSA (Thermo D12051) in maturation media for 30 minutes. Media was
632 replaced with fresh media (and fresh bafilomycin in the appropriate wells), and the red fluorescence and
633 bright field were imaged at 20x with an Incucyte (Sartorius) every hour for 24 hours.

634 Alternatively, astrocytes were seeded at 50K cells/well of a 12-well plate. Media changes were followed as
635 above. Cells were lifted to single-cell suspension with TrypLE Select 24 hours after the DQ-BSA pulse and
636 filtered into flow cytometry tubes with DAPI. Red fluorescence in live cells was analyzed with a BD Celesta
637 flow cytometer.

638 **LysoSensor by flow cytometry**

639 Astrocytes were seeded at 50,000 cells/well of a 12-well plate in AM. The following day, media was changed
640 to FBS-free maturation media (50% DMEM/F12, 50% Neurobasal, 1X B27 without Vitamin A, 1X N2, 1X
641 NEAA, 1X GlutaMAX, 1% penicillin-streptomycin), and cultured for 3 more days. Cells were incubated in 100
642 nM LysoSensor Green DND-189 (Thermo L7535) for 1 minute. Cells were washed and lifted to single cells
643 suspension with media changes followed as above. Cells were lifted to single-cell suspension with TrypLE
644 Select and filtered into flow cytometry tubes with DAPI. Green fluorescence in live cells was analyzed with a
645 BD Celesta flow cytometer.

646 **Live Imaging of α-Syn-HiLyte Uptake and Degradation**

647 Astrocytes were seeded 10,000 cells/well of a 96 well µClear plastic bottom plate (Greiner) in AM. The
648 following day, the media was changed to FBS-free maturation media (50% DMEM/F12, 50% Neurobasal, 1X
649 B27 without Vitamin A, 1X N2, 1X NEAA, 1X GlutaMAX, 1% penicillin-streptomycin), and cultured for 2 more
650 days. α-Syn HiLyte (AnaSpec AS-55457) was added to the media at a final concentration of 2 µg/mL and
651 nuclei were stained with 10 µg/mL Hoechst 33342. Images were acquired every 30-90 minutes for the first 6
652 hours on a Nikon AX R. At 24 h, the media was changed to fresh FBS-free maturation media to remove any
653 excess α-Syn. Images were acquired at 24 h and 48 h using the same parameters and laser settings.

654 **Live Imaging of BODIPY-Cholesterol**

655 Astrocytes were seeded 10,000 cells/well of a 96 well µClear plastic bottom plate (Greiner) in AM. The
656 following day, the media was changed to FBS-free maturation media (50% DMEM/F12, 50% Neurobasal, 1X
657 B27 without Vitamin A, 1X N2, 1X NEAA, 1X GlutaMAX, 1% penicillin-streptomycin), and cultured for 3 more
658 days. Astrocytes were incubated with 2 µM BODIPY-Cholesterol (Cayman 24618) for 2 hours. Cells were
659 then incubated with 10 µg/mL Hoechst 33342 for 10 minutes to stain nuclei and then washed. Media was
660 replaced with fresh media and cells were imaged using a CX7 High Content Screening Platform with a 20x
661 objective lens (Thermo; LUCPLFLN20x).

662 **Western blotting and dot blotting**

663 For Western blots, the protein concentration of each sample was measured using Pierce BCA Protein Assay
664 (Thermo Fisher). Volumes corresponding to 20 μg of protein for each sample were loaded into Criterion
665 Precast gels (BioRad), and a current of 120V was applied for approximately 60 min. The gel proteins were
666 transferred to a PVDF membrane using BioRad TransBlot Turbo Transfer System, fixed in 4% PFA for 40
667 min and blocked in 5% w/v non-fat milk in 0.1% Tween in TBS (TBST) for 1 hour. For antibodies against
668 phosphorylated proteins, blots were blocked in 5% w/v bovine serum albumin (BSA) in 0.1% TBST. Blots
669 were then incubated with primary antibodies diluted at 1:1000 in blocking buffer overnight at 4°C. Membranes
670 were washed in 0.1% TBST 3 times for 5 min each, incubated with secondary antibodies conjugates with
671 horseradish peroxidase for 2h at room temperature in blocking buffer, and exposed to chemiluminescence
672 activator before imaging using LI-COR Odyssey XF system. For dot blots, 3 mg of cell protein lysate or 3 ml
673 of media were added onto nitrocellulose membranes and allowed to dry. Blocking and antibody incubation
674 was performed as described for Western blots.

675 **Collection and treatment with conditioned media**

676 To generate neuron-conditioned media neurons were plated at ~150,000/cm2 on poly-L-ornithine and laminin
677 coated plates on day 7 of differentiation. Media was changed following the differentiation protocol described
678 above. Starting day 14 of differentiation, the media was collected, centrifuged at 2000xg for 5 minutes to
679 pellet debris, and stored at -20°C. Media was collected with each half media change, every 3-4 days.

680 To generate astrocyte conditioned media, astrocytes were plated at ~30,000/cm2 on 0.1% gelatin-coated
681 plates in AM. The following day, media was changed to either fresh neuron media (Neurobasal, 1x B-27, 1x
682 N-2, 1x MEM-NEAA, 1x GlutaMAX, 1% penicillin-streptomycin, 10ng/mL BDNF, 10ng/mL GDNF, 0.5 mM
683 dcAMP, 1ug/mL Laminin) supplemented with 10ng/mL CNTF or neuron conditioned media supplemented
684 with 10ng/mL CNTF. Media was collected, centrifuged at 2000xg for 5 minutes to pellet debris, and stored
685 at -20°C after 3 days.

686 To treat neurons with conditioned media, SNCA-A53T overexpressing neurons were plated at ~150,000/cm2
687 on poly-L-ornithine and laminin-coated 96-well μClear plates (Greiner) on day 7 of differentiation, following
688 the normal neuron differentiation protocol described above. On day 11 of differentiation, the media was
689 changed to conditioned media supplemented with 5 μg/mL doxycycline and 1 μg/mL laminin. Half media
690 changes with conditioned media supplemented with doxycycline and laminin were continued every 3-4 days
691 until day 25 of differentiation when cultures were fixed.

692 **Treatment with cholesterol-lowering drugs**

693 Astrocytes were seeded into 0.1% gelatin-coated 6 well plates in AM (ScienCell). After 2-3 days, the media
694 was changed to AM without FBS supplemented with cholesterol-lowering drugs or DMSO as a vehicle. After
695 4 days, cells were seeded for final assays in 0.1% gelatin-coated 96-well μClear plates (Greiner) in AM with
696 treatment. The following day, media was changed to FBS-free maturation media (50% DMEM/F12, 50%
697 Neurobasal, 1X B27 without Vitamin A, 1X N2, 1X NEAA, 1X GlutaMAX, 1% penicillin-streptomycin) with
698 treatment. Assays were started 2-3 days later, as described above. miBrains were treated with methyl-β-
699 cyclodextrin (concentration below) or DMSO from day 0 of assembly to day 18, with half-media changes
700 performed 3 times a week.

701 The following drug concentrations were used:
702 2-hydroxypropyl-β-cyclodextrin: 100 μM (Sigma C0926)

703 methyl-β-cyclodextrin: 100 μM (Cayman 21633)
704 atorvastatin: 50 nM (Sigma SML3030)
705 efavirenz: 10 μM (MedChemExpress HY10572)
706 LXR-623: 10 μM (MedChemExpress HY-10629)
707 T0901317: 10 μM (MedChemExpress HY-10626)

708 **Supplemental information**

709 Document S1. Figures S1-S4; Legends for Videos S1, S2, and S3
710 Video S1. Neurons with α-Synuclein pathological phenotypes within the miBrain; related to Figure 1
711 Video S2. *APOE3/3* astrocytes co-localize with neuronal-derived α-Synuclein; related to Figure 2
712 Video S3. *APOE4/4* reactive astrocytes poorly co-localize with neuronal-derived α-Synuclein; related to
713 Figure 2

714 **Figure Legends**

715 **Figure 1. *Induction of α-Syn intracellular inclusions in a multi-cellular integrated Brain (miBrain)***
716 ***tissue*. a**. Cartoon and representative images of our **m**ulticellular **i**ntegrated human **brain** (miBrain) tissue
717 generated from human iPSCs differentiated into six brain cell types, including neurons, glia, and vascular
718 cells. Four-week-old miBrains showing neurons (TUJ1, cyan) and vascular networks (PECAM-1, red). Scale
719 bar: 500 μm. Nuclei: blue. **b**. miBrains stained for specific markers of neurons (cyan; Neurofilament-H, TUJ1,
720 NGN2-sfGFP), astrocytes (green; S100b, AQP4), endothelial cells (red; PECAM-1), mural cells (green;
721 NG2), myelin (green; MBP), and microglia (green; IBA1). Scale bar: 50 μm, nuclei: blue. **c.** miBrains
722 containing neurons generated through direct iPSC reprograming via *NGN2* expression, with or without the
723 overexpression of *SNCA-A53T*. The tissue was cultured for a total of 18 days, with or without α-synuclein
724 PFFs added on day 4. Immunofluorescence for neuronal marker TUJ1 and for α-Syn phosphorylated at
725 Serine 129 (pS129) shows a robust expression of pS129-Syn in A53T neurons within the miBrains, but not
726 in WT tissue. Scale bar: 50 μm, nuclei: blue. Neuronal pS129 expression was significantly increased in
727 miBrains with A53T neurons. Exposure to PFFs exacerbated this effect. Bars represent means of pS129-
728 Syn$^+$ volume within TUJ1$^+$ neurons normalized to control WT. Error bars represent standard error (n = 4
729 biological replicates). P-values were calculated using a 2-way ANOVA followed by a Fisher's LSD test. **d**.
730 *SNCA-A53T* was fused to small folding green fluorescent protein (sfGFP). pS129-Syn$^+$ inclusions co-localize
731 with sfGFP expression in TUJ1$^+$ cells. Scale bar: 50 μm, nuclei: blue. **e**. Representative images depicting the
732 co-localization of SNCA-A53T-sfGFP (green) and neutral lipid marker Lipid Spot (magenta) in A53T miBrains,
733 or p-Syn (red) and Lipid Spot (cyan) in wild type and A53T miBrains cultured for two weeks. Arrowhead points
734 to a lipid droplet within a p-Syn$^+$ inclusion. The violin plot shows the percentage of sfGFP-SNCA volume
735 occupied by the overlapping signal of Lipid Spot. The sfGFP-SNCA volume overlapped at 5.2 % ± 0.7 with
736 lipid droplet marker Lipid Spot (mean ± standard error, n = 6 biological replicates). Dot plots represent the
737 median overlapping volume between p-Syn and Lipid Spot normalized by nuclei (n = 5-6 biological
738 replicates). P-values were calculated by Mann-Whitney test. Scale bar: 50 μm. **f.** Live imaging of SNCA-
739 A53T-sfGFP in cell bodies (i), neurites (ii), and varicose-like inclusions (iii). Scale bars: 25 μm (i, ii) and 15μm
740 (iii). Line graphs show the number of somatic and neuritic inclusions normalized by the sfGFP volume over
741 time (n = 4 biological replicates). Compared to WT, miBrains with A53T neurons had a significant increase
742 in the levels of lactate dehydrogenase (LDH) in the media, indicating cell death. Bars represent mean LDH
743 luminescence normalized to WT control, and error bars represent standard error (n = 4 biological replicates).
744 P-values were calculated using an unpaired t-test. Representative images of live tracking of SNCA-A53T-
745 sfGFP imaging and quantification at 2 and 22 weeks after miBrain assembly revealed a reduction in sfGFP
746 area between 2 and 22 weeks ($p < 0.0001$). Bars represent mean sfGFP volume. Error bars represent

747 standard error (n = 4 biological replicates). Scale bar: 100 µm. **g**. Representative images of miBrains with
748 A53T or WT neurons. The volume occupied by neurons (cyan; TUJ1) was significantly reduced in miBrains
749 with A53T neurons when compared with WT at 2 and 24 weeks. Bars represent TUJ1$^+$ volume and error
750 bars represent standard error (n = 3 biological replicates). P-values were calculated by 2-way ANOVA
751 followed by a Tukey test. Scale bar: 50 µm. **h.** Representative images of A53T miBrains stained for pS129
752 α-synuclein (red) and aggregated α-synuclein (cyan) 24 weeks after assembly. Bars represent the percent
753 volume of sfGFP-SNCA occupied by either pS129 α-Syn or aggregated α-synuclein staining. P-values were
754 calculated by Mann-Whitney test. Scale bar: 25 µm. *P < 0.05, **P < 0.01, ***P < 0.001, ****P < 0.0001

755 **Figure 2. *APOE4* increases the phosphorylation and aggregation of α-Syn via astrocytes. a.** Using
756 CRISPR-Cas9 on an *APOE3/3* iPSC line, we generated isogenic iPSCs harboring *APOE4/4* and
757 differentiated them into neurons with SNCA-A53T overexpression. We generated miBrains with *APOE3/3* or
758 *APOE4/4* isogenic cells. Representative images of phosphorylated α-Syn immunoreactivity in *APOE3/3* and
759 *APOE4/4* isogenic miBrains. Higher magnification panel depicts co-localized immunoreactivity between
760 pS129 (red), SNCA-A53T-sfGFP (green) and TUJ1 (magenta). Scale bars: 50 µm. *APOE4/4* miBrains had
761 significantly higher levels of pS129 (red) compared with *APOE3/3*. Bars represent mean values of percent
762 of sfGFP volume immunoreactive for phosphorylated α-Syn, normalized by *APOE3/3*. Error bars represent
763 standard error (n = 8 biological replicates). P-values were calculated using unpaired t-test. **b.** We generated
764 miBrains with *APOE3/3* or *APOE4/4* isogenic cells, including miBrains with one cell type at a time harboring
765 *APOE4/4* (yellow boxes) and the remaining cells *APOE3/3* (blue boxes). Representative images of
766 phosphorylated α-Syn in a combinatorial screen of *APOE3/3* and *APOE4/4* isogenic cell types. *APOE4/4*
767 and *APOE3/3* miBrains with *APOE4/4* astrocytes had equivalent levels of pS129 α-Syn (red). These levels
768 were significantly higher than in miBrains where all cells harbored *APOE3/3* or where any cell type except
769 astrocytes harbored *APOE4/4*. Bars represent mean values of percent of sfGFP volume immunoreactive for
770 phosphorylated α-Syn, and error bars represent standard error (n = 8 biological replicates per combination).
771 P-values were calculated using one-way ANOVA followed by a Dunnett's Multiple Comparisons Test. Scale
772 bar: 50 µm. **c.** Representative images of GFAP immunoreactivity in *APOE3/3* and *APOE4/4* miBrains. Scale
773 bar: 50 µm. *APOE4/4* miBrain astrocytes (GFAP$^+$) had reduced overlap with sfGFP-SNCA, increased
774 circularity and significantly higher levels of GFAP (magenta) compared with *APOE3/3*. Bars represent mean
775 values of GFAP volume and circularity and error bars represent standard error (n = 4 biological replicates).
776 P-values were calculated using unpaired t-test. *P < 0.05, **P < 0.01, ***P < 0.001, ****P < 0.0001

777 **Figure 3. Impaired lysosomal function of *APOE4/4* astrocytes seeds α-Syn phosphorylation in**
778 **neurons. a.** Pseudobulk analysis of human astrocytes (Haney et al. 2024) for *SNCA* expression. Bars
779 represent mean normalized psuedobulk gene count and error bars represent standard error (n = 8 APOE3/3
780 and n = 10 APOE4/4). P-value was calculated using unpaired t-test. **b** Western blots of *APOE3/3* and
781 *APOE4/4* astrocytes for total α-Syn protein and phosphorylated α-Syn protein. Total and phosphorylated
782 αSyn is increased in *APOE4/4* astrocytes. The expected band size of α-Syn monomers is approximately
783 18kDa. β-Actin was used as a loading control. (n = 3 replicates). **c.** Representative images of uptake and
784 degradation of exogenous, fluorescently labeled α-Syn (green). α-Syn was removed from the culture media
785 after 24 hours. *APOE3/3* astrocytes uptake and degrade αSyn more readily than APOE4/4 astrocytes. Data
786 points represent mean values of α-Syn-HiLyte mean intensity normalized to nuclei area and *APOE3/3* at the
787 first time point. Error bars represent standard error (n = 4 replicates). P-values were calculated using 2-way
788 ANOVA followed by a Tukey test. **d.** Left: DQ-BSA Red integrated intensity per cell confluency measured
789 over 24 hours on an Incucyte (Sartorius). BafilomycinA1 at 100nM was used as a control for non-lysosomal
790 proteolysis of DQ-BSA. Data points represent mean values and error bars represent standard error (n = 4
791 replicates). Right: DQ-BSA Green mean fluorescence intensity measured in DAPI negative cell population
792 by flow cytometry after 24 hours in two different isogenic iPSC lines. Bars represent mean values normalized

793 to APOE3/3 and error bars represent standard error (n = 3 replicates). P-values were calculated by unpaired
794 t-tests. **e.** Representative images of pS129 α-Syn (red) in *APOE3/3* and *APOE4/4* astrocytes after exposure
795 to fresh or conditioned neuron media. *APOE4/4* astrocytes have more pS129 a-Syn, which is further
796 increased upon incubation with neuronal media. Data points represent mean values of pS129 a-Syn
797 normalized to cell area (CD44; cyan), and error bars represent standard error (n = 6 replicates). P-values
798 were calculated using 2-way ANOVA followed by a Fisher's LSD test. **f.** Left: schematic of the experimental
799 paradigm generating "double conditioned media" from *APOE/3* or *APOE4/4* astrocytes previously exposed
800 to neuronal media. Center, right: Representative images of *SNCA*-A53T neurons treated with neuron
801 conditioned media or neuron and astrocyte conditioned media. Neurons treated with *APOE4/4* double
802 conditioned media showed significant increase in pS129 α-Syn compared to all other conditions. Bars
803 represent mean pS129 volume normalized by sfGFP volume. Error bars represent standard error (n = 5
804 replicates). P-values were calculated using 1-way ANOVA followed by a Tukey test. All scale bars = 50 μm.
805 *P < 0.05, **P < 0.01, ***P < 0.001, ****P < 0.0001.

806 **Figure 4. Reducing cholesterol improves *APOE4/4* astrocyte lysosomal and α-Syn homeostasis. a.**
807 Representative images of live astrocytes with BODIPY-cholesterol in two isogenic lines. *APOE4/4* astrocytes
808 have significantly more BODIPY-cholesterol staining than *APOE3/3* astrocytes. Bars represent BODIPY-
809 cholesterol mean intensity (green) normalized by Hoechst area (blue). Error bars represent standard error (n
810 = 3 replicates). P-values were calculated by unpaired t-tests. **b.** Representative images of BODIPY staining
811 in astrocytes treated with 2HβCD or MβCD. *APOE4/4* astrocytes have more BODIPY staining than *APOE3/3*
812 astrocytes, which is reduced after treatment. Bars represent BODIPY punctae (green) per cell number
813 (Hoechst; blue). Error bars represent standard error (n = 6 replicates). P-values were calculated by 2-way
814 ANOVA followed by a Tukey test. **c.** Top: DQ-BSA Red integrated intensity, in astrocytes with 2HβCD,
815 MβCD, atorvastatin, efavirenz, LXR-623, or T0901317 treatment, measured over 24 hours on an Incucyte
816 (Sartorius). Data points represent mean values and error bars represent standard error (n = 4 replicates).
817 Bottom: area under the curve calculation for DQ-BSA. Treatment of *APOE4/4* astrocytes with cyclodextrins,
818 but not other drugs, improved lysosomal proteolytic activity. Bars represent mean value and error bars
819 represent standard error (n = 4 replicates). P-values were calculated by 2-way ANOVA followed by a Tukey
820 test. **d.** Representative images of LysoTracker in astrocytes treated with 2HβCD or MβCD. Treatment with
821 cyclodextrins increased endolysosomal intensity. Bars represent LysoTracker mean intensity (magenta)
822 normalized by Hoechst area (blue). Error bars represent standard error (n = 5-6 replicates) P-values were
823 calculated by 2-way ANOVA followed by a Sidak test. **e.** Representative images of astrocytes treated with
824 cyclodextrins after a 24h incubation with fluorescently labeled α-Syn, in two isogenic lines. Cyclodextrin
825 treated astrocytes have increased α-Syn uptake compared to untreated *APOE4/4* astrocytes. Bars represent
826 a-Syn mean intensity (green) normalized by Hoechst area (blue). Error bars represent standard error (n = 6
827 replicates) P-values were calculated by 2-way ANOVA followed by a Tukey test. **f.** Representative images
828 of phosphorylated α-Syn in isogenic *APOE3/3* and *APOE4/4* miBrains. *APOE4/4* miBrains had significantly
829 higher levels of pS129 (red) than APOE3/3. These levels were significantly reduced in *APOE4/4* miBrains
830 treated with MβCD. Bars represent mean values of percent of sfGFP volume immunoreactive for
831 phosphorylated α-Syn and error bars represent standard error (n = 8 replicates). P-values were calculated
832 using two-way ANOVA followed by a Tukey test. All scale bars = 50μm. *P < 0.05, **P < 0.01, ***P < 0.001,
833 ****P < 0.0001.

834

835 **Extended Data Figure 1**. **miBrain cryopreservation and development of α-synuclein intracellular**
836 **inclusions**. **a.** Cartoon of the cryopreservation approach to preserve miBrains or smaller tissue units
837 (miVasC: microvascular combo; BBB: blood-brain barrier; JAM: just add missing cell type). **b.** Top: cell

838 viability upon thawing the cryopreserved tissue compared with fresh cells harvested and counted. Bars
839 represent cell viability (%), and error bars represent standard deviation (n = 3 biological replicates). Bottom:
840 quantification of the ratio between neurons and nuclei volume in 18 days-old thawed miBrain tissue from
841 three different batches. Bars represent ratio between TUJ1 and Hoechst volumes, and error bars represent
842 standard error (n = 3 batches with 4 to 8 biological replicates each). Representative images of two-week-old,
843 thawed tissue stained with markers of neurons (cyan; neurofilament), astrocytes (green; S100b, GFAP), and
844 endothelial cells (red; PECAM-1). Scale bars: 50 μm. **c.** Representative images of miBrains exposed to α-
845 synuclein PFFs for 48h and stained at two weeks. Scale bars: 500 μm and 50 μm on lower and higher
846 magnification, respectively. The levels of α-Syn phosphorylated at Serine 129 (pS129, red) were significantly
847 increased in miBrains exposed to PFFs. Bars represent the intensity of pS129-Syn immunostaining
848 normalized by nuclei and by control. Left graph shows the quantification of the experiment represented by
849 the images. Error bars represent standard error (n = 4 biological replicates). P-values were calculated using
850 an unpaired t-test. Right graph shows the quantification for the PFF treated group in three different
851 experiments (n = 4 biological replicates each). Error bars represent standard error. Only experiments 1 and
852 2 had mean levels higher than control. Point dispersion in the bar graphs display high variability. **d**.
853 Representative images of pS129 α-Syn in neurons generated from SNCA-A53T iPSCs, wild type (WT)
854 iPSCs, or SNCA-A53T iPSCs without the non-amyloid component (NAC) domain. SNCA-A53T neurons had
855 increased pS129 only in the presence of PFFs. Bars represent neuron volume, and error bars represent
856 standard error (n = 4 biological replicates). P-values were calculated by 2-way ANOVA followed by a Tukey
857 test. Scale bars: 50 μm. **e.** In A53T miBrains, the overlap between aggregated α-synuclein and Tom20 was
858 significantly increased. Dot plot represents the median volume of aggregated α-Syn overlapping with Tom20
859 (n = 4 biological replicates). P-value was calculated using a Mann-Whitney test. Scale bar: 25 μm. *P < 0.05,
860 **P < 0.01, ***P < 0.001, ****P < 0.0001.

861 **Extended Data Figure 2. Non-neuronal cells promote α-synuclein pathological phenotypes in APOE4**
862 **tissue. a.** Representative images of 2D *APOE3/3* and *APOE4/4* isogenic neuronal cultures overexpressing
863 SNCA-A53T-sfGFP and exposed to PFFs for 2 weeks. Scale bar: 50 μm. pS129 was increased in both
864 *APOE3/3* and *APOE4/4* SNCA-A53T neurons after exposure to PFFs when compared to WT controls. Bars
865 represent mean volume of phosphorylated α-Syn per β-III tubulin volume and normalized to control *APOE3/3*
866 neurons; error bars represent standard error (n = 4 biological replicates). **b.** Cartoon depicting the
867 experimental paradigm for generating isogenic *APOE3/3* and *APOE4/4* cells for miBrains. **c.** Cells were
868 harvested on the day of miBrain assembly, and a subset of the cells was plated in monocultures and fixed
869 after 24h. Representative images of *APOE3/3* and *APOE4/4* iPSC-derived cells stained for specific markers
870 (green) of each cell type. Nuclei: blue. Scale bar: 20 μm. Bars represent mean values of the area
871 immunoreactive for each cell marker normalized by nuclei and error bars represent standard error (n = 3
872 biological replicates). P-values were calculated using unpaired t-test. **d.** *APOE4/4* miBrains had significantly
873 higher levels of phosphorylated α-Syn outside the sfGFP volume compared with *APOE3/3*. Bars represent
874 mean values of percent of sfGFP volume outside the sfGFP volume, normalized by *APOE3/3*. Error bars
875 represent standard error (n = 8 biological replicates). P-values were calculated using unpaired t-test. **e.**
876 Representative images of *APOE3/3* and *APOE4/4* miBrains with WT or SNCA-A53T-sfGFP neurons. WT
877 miBrains were generated with isogenic *APOE3/3* or *APOE4/4* cells. A53T miBrains were generated with
878 A53T neurons that were differentiated from an iPSC line from an *APOE3/3* donor with familial Parkinson's
879 disease. All other cells were isogenic between each other except for the APOE locus. Scale bar: 50 μm. The
880 presence of the SNCA-A53T neurons significantly increased the levels of pS129-Syn, but this effect was
881 exacerbated when the non-neuronal cells harbored *APOE4/4*. Bars represent mean volume immunoreactive
882 for phosphorylated α-Syn per nuclei volume and normalized to *APOE3/3* miBrains with WT neurons. Error
883 bars represent standard error (n = 4 biological replicates). P- values were calculated using 2-way ANOVA

884 followed by a Fisher's LSD test. **f.** Representative images of *APOE3/3* and *APOE4/4* miBrains with isogenic
885 microglia and SNCA-A53T-sfGFP neurons. Scale bar: 50 μm. The presence of microglia in either APOE3/3
886 or APOE4/4 tissue did not significantly change the levels of pS129-Syn. Bars represent mean values of
887 percent of sfGFP volume immunoreactive for phosphorylated α-Syn, and error bars represent standard error
888 (n = 6 biological replicates per combination). P-values were calculated using 2-way ANOVA followed by a
889 Fisher's LSD test. *P < 0.05, **P < 0.01, ***P < 0.001, ****P < 0.0001.

890 **Extended Data Figure 3. Characterization of lysosomal function and α-Synuclein uptake and**
891 **accumulation in astrocytes. a.** RNAseq analysis of isogenic, iPSC derived astrocytes for SNCA expression.
892 Bars represent mean normalized counts and error bars represent standard error (n = 3 replicates). P-value
893 was calculated by unpaired t-test. **b.** Western blots of *APOE3/3* and *APOE4/4* astrocytes for total α-Syn
894 protein and phosphorylated α-Syn protein. Total and phosphorylated αSyn is increased in *APOE4/4*
895 astrocytes. The expected band size of α-Syn monomers is approximately 18kDa. β-Actin was used as a
896 loading control. (n = 3 replicates). **c.** Representative images of astrocytes with α-Syn-HiLyte (green) after 24
897 hours of uptake and 24 hours of degradation after treatment with BafilomycinA1 and MG-132. αSyn
898 degradation is only affected by lysosomal disruption in BafilomycinA1. Bars represent the mean α-Syn-HiLyte
899 intensity per nuclei area, normalized to control astrocytes. Error bars represent standard error (n = 5
900 replicates). P-values were calculated by one-way ANOVA followed by Tukey test. **d.** Representative images
901 of LAMP1 immunostaining (magenta) in two different isogenic iPSC lines. APOE4/4 astrocytes have
902 significantly less $LAMP1^+$ lysosomes. Bars represent mean intensity per nuclei area normalized to *APOE3/3*.
903 Error bars represent standard error (n = 4 replicates). P-values were calculated using unpaired t-tests. **e.**
904 LysoSensor mean fluorescence intensity after 1 minute incubation measured by flow cytometry in DAPI
905 negative cells in three different isogenic iPSC lines. *APOE4/4* astrocytes have significantly reduced
906 LysoSensor signal compared to *APOE3/3* astrocytes. Bars represent mean values normalized to APOE3/3
907 and error bars represent standard error (n = 3 replicates). P-values were calculated using unpaired t-tests.
908 **f.** Top: Schematic of the experimental paradigm generating astrocyte conditioned media from *APOE3/3* and
909 *APOE4/4* astrocytes. Bottom: Representative images of *SNCA*-A53T neurons treated with conditioned media
910 from naïve *APOE3/3* or *APOE4/4* astrocytes, or with fresh neuron media. There was no differential effect
911 between conditions. Bars represent mean pS129 volume normalized by sfGFP volume. Error bars represent
912 standard error (n = 6 replicates). P-values were calculated using 1-way ANOVA followed by a Tukey test. **g**.
913 Dot blots of *SNCA*-A53T conditioned media or double conditioned media from SNCA-A53T neurons and
914 isogenic *APOE3/3* or *APOE4/4* astrocytes for total αSyn, phosphorylated αSyn, and aggregated αSyn. All
915 dots were on one blot; the image was cropped to fit for the figure. Bars represent mean intensity and error
916 bars represent standard error (n = 4 replicates). P-values were calculated by unpaired, t-tests. All scale bars
917 = 50 μm. *P < 0.05, **P < 0.01, ***P < 0.001, ****P < 0.0001.

918 **Extended Data Figure 4. MβCD treatment in *APOE4/4* astrocytes improves lysosomal uptake of α-**
919 **Synuclein. a.** Volcano plot of *APOE4/4* vs. *APOE3/3* astrocytes showing DEGs (p val adj < 0.5, abs(logFC
920 > 0.5). Top 10 Gene Ontology (GO) upregulated (red) and downregulated (blue) pathways ranked by
921 adjusted p-value. Genes highlighted in the volcano plot correspond to GO terms related to lipid metabolism,
922 including "fatty acid oxidation", "cellular response to fatty acid", "regulation of lipid storage", "monocarboxylic
923 acid transport", "fatty acid transport", "cholesterol transfer activity", and "cholesterol metabolic process". **b.**
924 Left: DQ-BSA Red integrated intensity in astrocytes with 2HβCD or MβCD treatment, measured over 24
925 hours on an Incucyte (Sartorius) in a second isogenic donor line. Data points represent mean values and
926 error bars represent standard error (n = 4 replicates). Right: Area under the curve calculation for DQ-BSA.
927 Treatment of *APOE4/4* astrocytes with MβCD improved lysosomal proteolytic activity in a second donor line.
928 Bars represent mean value and error bars represent standard error (n = 4 replicates). P-values were
929 calculated by 2-way ANOVA followed by a Tukey test. **c.** Representative images of LysoTracker in astrocytes

930 treated with cyclodextrins in a second isogenic donor line. Treatment with cyclodextrins increased
931 endolysosomal area. Bars represent LysoTracker mean intensity (magenta) normalized by Hoechst area
932 (blue). Error bars represent standard error (n = 5-6 replicates) P-values were calculated by 2-way ANOVA
933 followed by a Sidak test. **d.** Representative images of astrocytes treated with cyclodextrins after a 24h
934 incubation with fluorescently labeled α-Syn in a second isogenic donor line. Cyclodextrin treated astrocytes
935 have increased α-Syn uptake compared to untreated *APOE4/4* astrocytes. Bars represent α-Syn mean
936 intensity (green) normalized by Hoechst area (blue). Error bars represent standard error (n = 6 replicates) P-
937 values were calculated by 2-way ANOVA followed by a Tukey test. **e.** Representative images of fluorescently
938 labeled α-Syn co-localized with endolysosomes in astrocytes treated with cyclodextrins. Cyclodextrin treated
939 astrocytes had increased co-localization between α-Syn and lysosomes compared to untreated *APOE4/4,*
940 indicative of improved α-Syn uptake. Bars represent mean Mander's coefficient M2 (amount of a-Syn signal
941 in overlapping LysoTracker). Error bars represent standard error (n = 8 replicates). P-values were calculated
942 by 2-way ANOVA followed by a Fisher's LSD test. All scale bars = 50μm. *P < 0.05, **P < 0.01, ***P < 0.001,
943 ****P < 0.0001.

944 **Extended Data Video 1.** Neurons with α-synuclein pathological phenotypes within the miBrain. 3D rendering
945 with animated orthogonal projection of SNCA-A53T neurons within the miBrain. Green: SNCA-A53T-sfGFP;
946 red: pS129 α-Syn; magenta: TUJ1, blue: Hoechst.

947 **Extended Data Video 2. APOE3/3 astrocytes co-localize with neuronal-derived α-synuclein.** 3D
948 rendering with animated orthogonal projection of astrocytes within an *APOE3/3* miBrain. Astrocytes display
949 elongated morphology along neuronal networks. Green: SNCA-A53T-sfGFP; magenta: GFAP, blue:
950 Hoechst.

951 **Extended Data Video 3. *APOE4/4* reactive astrocytes poorly co-localize with neuronal-derived α-**
952 **synuclein.** 3D rendering with animated orthogonal projection of astrocytes within an *APOE4/4* miBrain.
953 Astrocytes display amoeboid morphology not aligned with neuronal networks. Green: SNCA-A53T-sfGFP;
954 magenta: GFAP, blue: Hoechst.

References

1. Hardy JA, Higgins GA. Alzheimer's disease: the amyloid cascade hypothesis. *Science*. Apr 10 1992;256(5054):184-5. doi:10.1126/science.1566067

2. Kotzbauer PT, Trojanowsk JQ, Lee VM. Lewy body pathology in Alzheimer's disease. *J Mol Neurosci*. Oct 2001;17(2):225-32. doi:10.1385/jmn:17:2:225

3. Uchikado H, Lin WL, DeLucia MW, Dickson DW. Alzheimer disease with amygdala Lewy bodies: a distinct form of alpha-synucleinopathy. *J Neuropathol Exp Neurol*. Jul 2006;65(7):685-97. doi:10.1097/01.jnen.0000225908.90052.07

4. Popescu A, Lippa CF, Lee VM, Trojanowski JQ. Lewy bodies in the amygdala: increase of alpha-synuclein aggregates in neurodegenerative diseases with tau-based inclusions. *Arch Neurol*. Dec 2004;61(12):1915-9. doi:10.1001/archneur.61.12.1915

5. Lippa CF, Fujiwara H, Mann DM, et al. Lewy bodies contain altered alpha-synuclein in brains of many familial Alzheimer's disease patients with mutations in presenilin and amyloid precursor protein genes. *Am J Pathol*. Nov 1998;153(5):1365-70. doi:10.1016/s0002-9440(10)65722-7

6. Hansen LA, Masliah E, Galasko D, Terry RD. Plaque-only Alzheimer disease is usually the lewy body variant, and vice versa. *J Neuropathol Exp Neurol*. Nov 1993;52(6):648-54. doi:10.1097/00005072-199311000-00012

7. Iwai A, Masliah E, Sundsmo MP, et al. The synaptic protein NACP is abnormally expressed during the progression of Alzheimer's disease. *Brain Res*. May 13 1996;720(1-2):230-4. doi:10.1016/0006-8993(96)00014-5

8. Hamilton RL. Lewy bodies in Alzheimer's disease: a neuropathological review of 145 cases using alpha-synuclein immunohistochemistry. *Brain Pathol*. Jul 2000;10(3):378-84. doi:10.1111/j.1750-3639.2000.tb00269.x

9. Arai Y, Yamazaki M, Mori O, Muramatsu H, Asano G, Katayama Y. Alpha-synuclein-positive structures in cases with sporadic Alzheimer's disease: morphology and its relationship to tau aggregation. *Brain Res*. Jan 12 2001;888(2):287-296. doi:10.1016/s0006-8993(00)03082-1

10. Marui W, Iseki E, Ueda K, Kosaka K. Occurrence of human alpha-synuclein immunoreactive neurons with neurofibrillary tangle formation in the limbic areas of patients with Alzheimer's disease. *J Neurol Sci*. Mar 15 2000;174(2):81-4. doi:10.1016/s0022-510x(99)00327-5

11. Olichney JM, Galasko D, Salmon DP, et al. Cognitive decline is faster in Lewy body variant than in Alzheimer's disease. *Neurology*. Aug 1998;51(2):351-7. doi:10.1212/wnl.51.2.351

12. Chung EJ, Babulal GM, Monsell SE, Cairns NJ, Roe CM, Morris JC. Clinical Features of Alzheimer Disease With and Without Lewy Bodies. *JAMA Neurol*. Jul 2015;72(7):789-96. doi:10.1001/jamaneurol.2015.0606

13. Capouch SD, Farlow MR, Brosch JR. A Review of Dementia with Lewy Bodies' Impact, Diagnostic Criteria and Treatment. *Neurol Ther*. Dec 2018;7(2):249-263. doi:10.1007/s40120-018-0104-1

14. Guerreiro R, Ross OA, Kun-Rodrigues C, et al. Investigating the genetic architecture of dementia with Lewy bodies: a two-stage genome-wide association study. *Lancet Neurol*. Jan 2018;17(1):64-74. doi:10.1016/S1474-4422(17)30400-3

15. Tsuang D, Leverenz JB, Lopez OL, et al. APOE epsilon4 increases risk for dementia in pure synucleinopathies. *JAMA Neurol*. Feb 2013;70(2):223-8. doi:10.1001/jamaneurol.2013.600

16. Luk KC, Kehm V, Carroll J, et al. Pathological alpha-synuclein transmission initiates Parkinson-like neurodegeneration in nontransgenic mice. *Science*. Nov 16 2012;338(6109):949-53. doi:10.1126/science.1227157

17. Chung HK, Ho HA, Perez-Acuna D, Lee SJ. Modeling alpha-Synuclein Propagation with Preformed Fibril Injections. *J Mov Disord*. Sep 2019;12(3):139-151. doi:10.14802/jmd.19046

18. Volpicelli-Daley LA, Luk KC, Lee VM. Addition of exogenous alpha-synuclein preformed fibrils to primary neuronal cultures to seed recruitment of endogenous alpha-synuclein to Lewy body and Lewy neurite-like aggregates. *Nat Protoc*. Sep 2014;9(9):2135-46. doi:10.1038/nprot.2014.143

19. Volpicelli-Daley LA, Luk KC, Patel TP, et al. Exogenous alpha-synuclein fibrils induce Lewy body pathology leading to synaptic dysfunction and neuron death. *Neuron*. Oct 6 2011;72(1):57-71. doi:10.1016/j.neuron.2011.08.033

20. Pediaditakis I, Kodella KR, Manatakis DV, et al. Modeling alpha-synuclein pathology in a human brain-chip to assess blood-brain barrier disruption. *Nat Commun*. Oct 8 2021;12(1):5907. doi:10.1038/s41467-021-26066-5

21. Jia L, Liu Y, Wang W, et al. Molecular Mediation of Prion-like alpha-Synuclein Fibrillation from Toxic PFFs to Nontoxic Species. *ACS Appl Bio Mater*. Sep 21 2020;3(9):6096-6102. doi:10.1021/acsabm.0c00684

22. Jan A, Goncalves NP, Vaegter CB, Jensen PH, Ferreira N. The Prion-Like Spreading of Alpha-Synuclein in Parkinson's Disease: Update on Models and Hypotheses. *Int J Mol Sci*. Aug 3 2021;22(15)doi:10.3390/ijms22158338

23. Bousset L, Brundin P, Bockmann A, Meier B, Melki R. An Efficient Procedure for Removal and Inactivation of Alpha-Synuclein Assemblies from Laboratory Materials. *J Parkinsons Dis*. 2016;6(1):143-51. doi:10.3233/JPD-150691

24. Duval K, Grover H, Han LH, et al. Modeling Physiological Events in 2D vs. 3D Cell Culture. *Physiology (Bethesda)*. Jul 2017;32(4):266-277. doi:10.1152/physiol.00036.2016

25. Sierksma A, Escott-Price V, De Strooper B. Translating genetic risk of Alzheimer's disease into mechanistic insight and drug targets. *Science*. Oct 2 2020;370(6512):61-66. doi:10.1126/science.abb8575

26. Lancaster MA, Renner M, Martin CA, et al. Cerebral organoids model human brain development and microcephaly. *Nature*. Sep 19 2013;501(7467):373-9. doi:10.1038/nature12517

27. Stanton AE, Bubnys A, Agbas E, et al. Engineered 3D Immuno-Glial-Neurovascular Human Brain Model. *bioRxiv*. Aug 17 2023;doi:10.1101/2023.08.15.553453

28. Mazzulli JR, Zunke F, Isacson O, Studer L, Krainc D. alpha-Synuclein-induced lysosomal dysfunction occurs through disruptions in protein trafficking in human midbrain synucleinopathy models. *Proc Natl Acad Sci U S A*. Feb 16 2016;113(7):1931-6. doi:10.1073/pnas.1520335113

29. Lam I, Ndayisaba A, Lewis AJ, et al. Rapid iPSC inclusionopathy models shed light on formation, consequence, and molecular subtype of alpha-synuclein inclusions. *Neuron*. Jul 23 2024;doi:10.1016/j.neuron.2024.06.002

30. Zhang Y, Pak C, Han Y, et al. Rapid single-step induction of functional neurons from human pluripotent stem cells. *Neuron*. Jun 5 2013;78(5):785-98. doi:10.1016/j.neuron.2013.05.029

31. Chambers SM, Fasano CA, Papapetrou EP, Tomishima M, Sadelain M, Studer L. Highly efficient neural conversion of human ES and iPS cells by dual inhibition of SMAD signaling. *Nat Biotechnol*. Mar 2009;27(3):275-80. doi:10.1038/nbt.1529

32. Tcw J, Wang M, Pimenova AA, et al. An Efficient Platform for Astrocyte Differentiation from Human Induced Pluripotent Stem Cells. *Stem Cell Reports*. Aug 8 2017;9(2):600-614. doi:10.1016/j.stemcr.2017.06.018

1042 33. Blanchard JW, Bula M, Davila-Velderrain J, et al. Reconstruction of the human blood-brain barrier in
1043 vitro reveals a pathogenic mechanism of APOE4 in pericytes. *Nat Med*. Jun 2020;26(6):952-963.
1044 doi:10.1038/s41591-020-0886-4

1045 34. Mesentier-Louro LA, Suhy N, Broekaart D, Bula M, Pereira AC, Blanchard JW. Modeling the Blood-
1046 Brain Barrier Using Human-Induced Pluripotent Stem Cells. *Methods Mol Biol*. 2023;2683:135-151.
1047 doi:10.1007/978-1-0716-3287-1_11

1048 35. Goldman C, Suhy N, Schwarz JE, et al. Reconstruction of the Blood-Brain Barrier In Vitro to Model and
1049 Therapeutically Target Neurological Disease. *J Vis Exp*. Oct 20 2023;(200)doi:10.3791/65921

1050 36. Wang K, Lin RZ, Hong X, et al. Robust differentiation of human pluripotent stem cells into endothelial
1051 cells via temporal modulation of ETV2 with modified mRNA. *Sci Adv*. Jul 2020;6(30):eaba7606.
1052 doi:10.1126/sciadv.aba7606

1053 37. Patsch C, Challet-Meylan L, Thoma EC, et al. Generation of vascular endothelial and smooth muscle
1054 cells from human pluripotent stem cells. *Nat Cell Biol*. Aug 2015;17(8):994-1003. doi:10.1038/ncb3205

1055 38. Douvaras P, Fossati V. Generation and isolation of oligodendrocyte progenitor cells from human
1056 pluripotent stem cells. *Nat Protoc*. Aug 2015;10(8):1143-54. doi:10.1038/nprot.2015.075

1057 39. McQuade A, Coburn M, Tu CH, Hasselmann J, Davtyan H, Blurton-Jones M. Development and
1058 validation of a simplified method to generate human microglia from pluripotent stem cells. *Mol*
1059 *Neurodegener*. Dec 22 2018;13(1):67. doi:10.1186/s13024-018-0297-x

1060 40. Quadrato G, Nguyen T, Macosko EZ, et al. Cell diversity and network dynamics in photosensitive
1061 human brain organoids. *Nature*. May 4 2017;545(7652):48-53. doi:10.1038/nature22047

1062 41. Anderson JP, Walker DE, Goldstein JM, et al. Phosphorylation of Ser-129 is the dominant pathological
1063 modification of alpha-synuclein in familial and sporadic Lewy body disease. *J Biol Chem*. Oct 6
1064 2006;281(40):29739-52. doi:10.1074/jbc.M600933200

1065 42. Fujiwara H, Hasegawa M, Dohmae N, et al. alpha-Synuclein is phosphorylated in synucleinopathy
1066 lesions. *Nat Cell Biol*. Feb 2002;4(2):160-4. doi:10.1038/ncb748

1067 43. Braak H, Del Tredici K, Rub U, de Vos RA, Jansen Steur EN, Braak E. Staging of brain pathology
1068 related to sporadic Parkinson's disease. *Neurobiol Aging*. Mar-Apr 2003;24(2):197-211.
1069 doi:10.1016/s0197-4580(02)00065-9

1070 44. Narhi L, Wood SJ, Steavenson S, et al. Both familial Parkinson's disease mutations accelerate alpha-
1071 synuclein aggregation. *J Biol Chem*. Apr 2 1999;274(14):9843-6. doi:10.1074/jbc.274.14.9843

1072 45. Giasson BI, Duda JE, Quinn SM, Zhang B, Trojanowski JQ, Lee VM. Neuronal alpha-synucleinopathy
1073 with severe movement disorder in mice expressing A53T human alpha-synuclein. *Neuron*. May 16
1074 2002;34(4):521-33. doi:10.1016/s0896-6273(02)00682-7

1075 46. Altay MF, Kumar ST, Burtscher J, et al. Development and validation of an expanded antibody toolset
1076 that captures alpha-synuclein pathological diversity in Lewy body diseases. *NPJ Parkinsons Dis*. Dec
1077 7 2023;9(1):161. doi:10.1038/s41531-023-00604-y

1078 47. Gai WP, Yuan HX, Li XQ, Power JT, Blumbergs PC, Jensen PH. In situ and in vitro study of
1079 colocalization and segregation of alpha-synuclein, ubiquitin, and lipids in Lewy bodies. *Exp Neurol*. Dec
1080 2000;166(2):324-33. doi:10.1006/exnr.2000.7527

1081 48. Reeve AK, Park TK, Jaros E, et al. Relationship between mitochondria and alpha-synuclein: a study of
1082 single substantia nigra neurons. *Arch Neurol*. Mar 2012;69(3):385-93.
1083 doi:10.1001/archneurol.2011.2675

1084 49. Wang X, Becker K, Levine N, et al. Pathogenic alpha-synuclein aggregates preferentially bind to
1085 mitochondria and affect cellular respiration. *Acta Neuropathol Commun*. Mar 14 2019;7(1):41.
1086 doi:10.1186/s40478-019-0696-4

1087 50. Cookson MR. alpha-Synuclein and neuronal cell death. *Mol Neurodegener*. Feb 4 2009;4:9.
1088 doi:10.1186/1750-1326-4-9

1089 51. Calabresi P, Mechelli A, Natale G, Volpicelli-Daley L, Di Lazzaro G, Ghiglieri V. Alpha-synuclein in
1090 Parkinson's disease and other synucleinopathies: from overt neurodegeneration back to early synaptic
1091 dysfunction. *Cell Death Dis*. Mar 1 2023;14(3):176. doi:10.1038/s41419-023-05672-9

1092 52. Zhao N, Liu CC, Qiao W, Bu G. Apolipoprotein E, Receptors, and Modulation of Alzheimer's Disease.
1093 *Biol Psychiatry*. Feb 15 2018;83(4):347-357. doi:10.1016/j.biopsych.2017.03.003

1094 53. Yamazaki Y, Zhao N, Caulfield TR, Liu CC, Bu G. Apolipoprotein E and Alzheimer disease:
1095 pathobiology and targeting strategies. *Nat Rev Neurol*. Sep 2019;15(9):501-518. doi:10.1038/s41582-
1096 019-0228-7

1097 54. Davis AA, Inman CE, Wargel ZM, et al. APOE genotype regulates pathology and disease progression
1098 in synucleinopathy. *Sci Transl Med*. Feb 5 2020;12(529)doi:10.1126/scitranslmed.aay3069

1099 55. Zhao N, Attrebi ON, Ren Y, et al. APOE4 exacerbates alpha-synuclein pathology and related toxicity
1100 independent of amyloid. *Sci Transl Med*. Feb 5 2020;12(529)doi:10.1126/scitranslmed.aay1809

1101 56. Zhao J, Lu W, Ren Y, et al. Apolipoprotein E regulates lipid metabolism and alpha-synuclein pathology
1102 in human iPSC-derived cerebral organoids. *Acta Neuropathol*. Nov 2021;142(5):807-825.
1103 doi:10.1007/s00401-021-02361-9

1104 57. Lin YT, Seo J, Gao F, et al. APOE4 Causes Widespread Molecular and Cellular Alterations Associated
1105 with Alzheimer's Disease Phenotypes in Human iPSC-Derived Brain Cell Types. *Neuron*. Jun 27
1106 2018;98(6):1141-1154 e7. doi:10.1016/j.neuron.2018.05.008

1107 58. Tcw J, Qian L, Pipalia NH, et al. Cholesterol and matrisome pathways dysregulated in astrocytes and
1108 microglia. *Cell*. Jun 23 2022;185(13):2213-2233 e25. doi:10.1016/j.cell.2022.05.017

1109 59. Choi I, Zhang Y, Seegobin SP, et al. Microglia clear neuron-released alpha-synuclein via selective
1110 autophagy and prevent neurodegeneration. *Nat Commun*. Mar 13 2020;11(1):1386.
1111 doi:10.1038/s41467-020-15119-w

1112 60. Scheiblich H, Dansokho C, Mercan D, et al. Microglia jointly degrade fibrillar alpha-synuclein cargo by
1113 distribution through tunneling nanotubes. *Cell*. Sep 30 2021;184(20):5089-5106 e21.
1114 doi:10.1016/j.cell.2021.09.007

1115 61. Lee HJ, Suk JE, Patrick C, et al. Direct transfer of alpha-synuclein from neuron to astroglia causes
1116 inflammatory responses in synucleinopathies. *J Biol Chem*. Mar 19 2010;285(12):9262-72.
1117 doi:10.1074/jbc.M109.081125

1118 62. Loria F, Vargas JY, Bousset L, et al. alpha-Synuclein transfer between neurons and astrocytes
1119 indicates that astrocytes play a role in degradation rather than in spreading. *Acta Neuropathol*. Nov
1120 2017;134(5):789-808. doi:10.1007/s00401-017-1746-2

1121 63. Tsunemi T, Perez-Rosello T, Ishiguro Y, et al. Increased Lysosomal Exocytosis Induced by Lysosomal
1122 Ca(2+) Channel Agonists Protects Human Dopaminergic Neurons from alpha-Synuclein Toxicity. *J*
1123 *Neurosci*. Jul 17 2019;39(29):5760-5772. doi:10.1523/JNEUROSCI.3085-18.2019

1124 64. Haney MS, Palovics R, Munson CN, et al. APOE4/4 is linked to damaging lipid droplets in Alzheimer's
1125 disease microglia. *Nature*. Apr 2024;628(8006):154-161. doi:10.1038/s41586-024-07185-7

1126 65. Stefanis L, Emmanouilidou E, Pantazopoulou M, Kirik D, Vekrellis K, Tofaris GK. How is alpha-
1127 synuclein cleared from the cell? *J Neurochem*. Sep 2019;150(5):577-590. doi:10.1111/jnc.14704

1128 66. Konings SC, Torres-Garcia L, Martinsson I, Gouras GK. Astrocytic and Neuronal Apolipoprotein E
1129 Isoforms Differentially Affect Neuronal Excitability. *Front Neurosci*. 2021;15:734001.
1130 doi:10.3389/fnins.2021.734001

1131 67. Pfrieger FW. Role of cholesterol in synapse formation and function. *Biochim Biophys Acta*. Mar 10
1132 2003;1610(2):271-80. doi:10.1016/s0005-2736(03)00024-5

1133 68. Lane-Donovan C, Philips GT, Herz J. More than cholesterol transporters: lipoprotein receptors in CNS
1134 function and neurodegeneration. *Neuron*. Aug 20 2014;83(4):771-87.
1135 doi:10.1016/j.neuron.2014.08.005

1136 69. Jeong W, Lee H, Cho S, Seo J. ApoE4-Induced Cholesterol Dysregulation and Its Brain Cell Type-
1137 Specific Implications in the Pathogenesis of Alzheimer's Disease. *Mol Cells*. Nov 30 2019;42(11):739-
1138 746. doi:10.14348/molcells.2019.0200

1139 70. Lee H, Cho S, Kim MJ, et al. ApoE4-dependent lysosomal cholesterol accumulation impairs
1140 mitochondrial homeostasis and oxidative phosphorylation in human astrocytes. *Cell Rep*. Oct 31
1141 2023;42(10):113183. doi:10.1016/j.celrep.2023.113183

1142 71. Liddelow SA, Guttenplan KA, Clarke LE, et al. Neurotoxic reactive astrocytes are induced by activated
1143 microglia. *Nature*. Jan 26 2017;541(7638):481-487. doi:10.1038/nature21029

1144 72. Chen Y, Qin C, Huang J, et al. The role of astrocytes in oxidative stress of central nervous system: A
1145 mixed blessing. *Cell Prolif*. Mar 2020;53(3):e12781. doi:10.1111/cpr.12781

1146 73. de Leeuw SM, Kirschner AWT, Lindner K, et al. APOE2, E3, and E4 differentially modulate cellular
1147 homeostasis, cholesterol metabolism, and inflammatory response in isogenic iPSC-derived astrocytes.
1148 *Stem Cell Reports*. Jan 11 2022;17(1):110-126. doi:10.1016/j.stemcr.2021.11.007

1149 74. Strauss K, Goebel C, Runz H, et al. Exosome secretion ameliorates lysosomal storage of cholesterol
1150 in Niemann-Pick type C disease. *J Biol Chem*. Aug 20 2010;285(34):26279-88.
1151 doi:10.1074/jbc.M110.134775

1152 75. Stykel MG, Humphries KM, Kamski-Hennekam E, et al. alpha-Synuclein mutation impairs processing
1153 of endomembrane compartments and promotes exocytosis and seeding of alpha-synuclein pathology.
1154 *Cell Rep*. May 11 2021;35(6):109099. doi:10.1016/j.celrep.2021.109099

1155 76. Sharma R, Hastings C, Staretz-Chacham O, et al. Long-term administration of intravenous Trappsol(R)
1156 Cyclo (HP-beta-CD) results in clinical benefits and stabilization or slowing of disease progression in
1157 patients with Niemann-Pick disease type C1: Results of an international 48-week Phase I/II trial. *Mol*
1158 *Genet Metab Rep*. Sep 2023;36:100988. doi:10.1016/j.ymgmr.2023.100988

1159 77. Min JO, Ho HA, Lee W, et al. Statins suppress cell-to-cell propagation of alpha-synuclein by lowering
1160 cholesterol. *Cell Death Dis*. Jul 27 2023;14(7):474. doi:10.1038/s41419-023-05977-9

1161 78. Oveisgharan S, Yu L, Barnes LL, et al. Association of Statins With Cerebral Atherosclerosis and
1162 Incident Parkinsonism in Older Adults. *Neurology*. May 10 2022;98(19):e1976-e1984.
1163 doi:10.1212/WNL.0000000000200182

1164 79. Stevens KN, Creanor S, Jeffery A, et al. Evaluation of Simvastatin as a Disease-Modifying Treatment
1165 for Patients With Parkinson Disease: A Randomized Clinical Trial. *JAMA Neurol*. Dec 1
1166 2022;79(12):1232-1241. doi:10.1001/jamaneurol.2022.3718

1167 80. Qian T, Maguire SE, Canfield SG, et al. Directed differentiation of human pluripotent stem cells to blood-
1168 brain barrier endothelial cells. *Sci Adv*. Nov 2017;3(11):e1701679. doi:10.1126/sciadv.1701679

1169 81. Douvaras P, Wang J, Zimmer M, et al. Efficient generation of myelinating oligodendrocytes from primary
1170 progressive multiple sclerosis patients by induced pluripotent stem cells. *Stem Cell Reports*. Aug 12
1171 2014;3(2):250-9. doi:10.1016/j.stemcr.2014.06.012

1172 82. McQuade A, Blurton-Jones M. Human Induced Pluripotent Stem Cell-Derived Microglia (hiPSC-
1173 Microglia). In: Nagy A, Turksen K, eds. *Induced Pluripotent Stem (iPS) Cells: Methods and Protocols*.
1174 Springer US; 2022:473-482.

1175 83. Giasson BI, Murray IV, Trojanowski JQ, Lee VM. A hydrophobic stretch of 12 amino acid residues in
1176 the middle of alpha-synuclein is essential for filament assembly. *J Biol Chem*. Jan 26 2001;276(4):2380-
1177 6. doi:10.1074/jbc.M008919200

1178 84. Hao Y, Hao S, Andersen-Nissen E, et al. Integrated analysis of multimodal single-cell data. *Cell*. Jun
1179 24 2021;184(13):3573-3587 e29. doi:10.1016/j.cell.2021.04.048

1180 85. McGinnis CS, Murrow LM, Gartner ZJ. DoubletFinder: Doublet Detection in Single-Cell RNA
1181 Sequencing Data Using Artificial Nearest Neighbors. *Cell Syst*. Apr 24 2019;8(4):329-337 e4.
1182 doi:10.1016/j.cels.2019.03.003

1183 86. Love MI, Huber W, Anders S. Moderated estimation of fold change and dispersion for RNA-seq data
1184 with DESeq2. *Genome Biol*. 2014;15(12):550. doi:10.1186/s13059-014-0550-8

1185

Figure 1

miBrain System

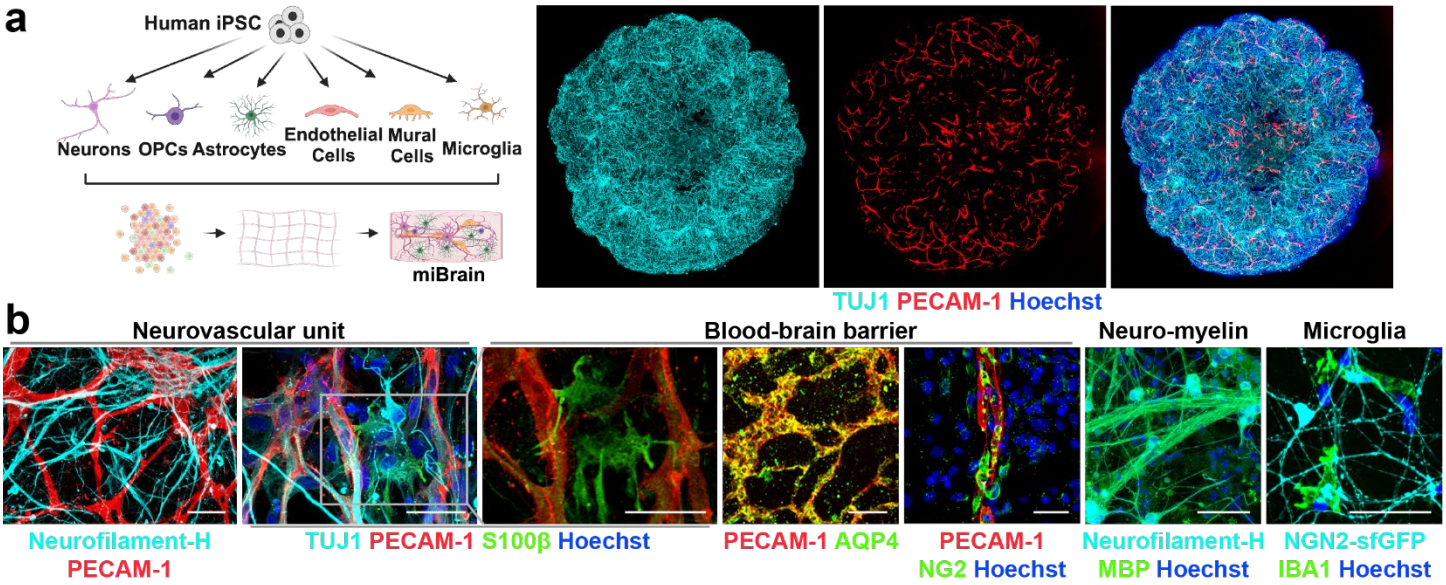

Synuclein Pathological Phenotypes in the miBrain

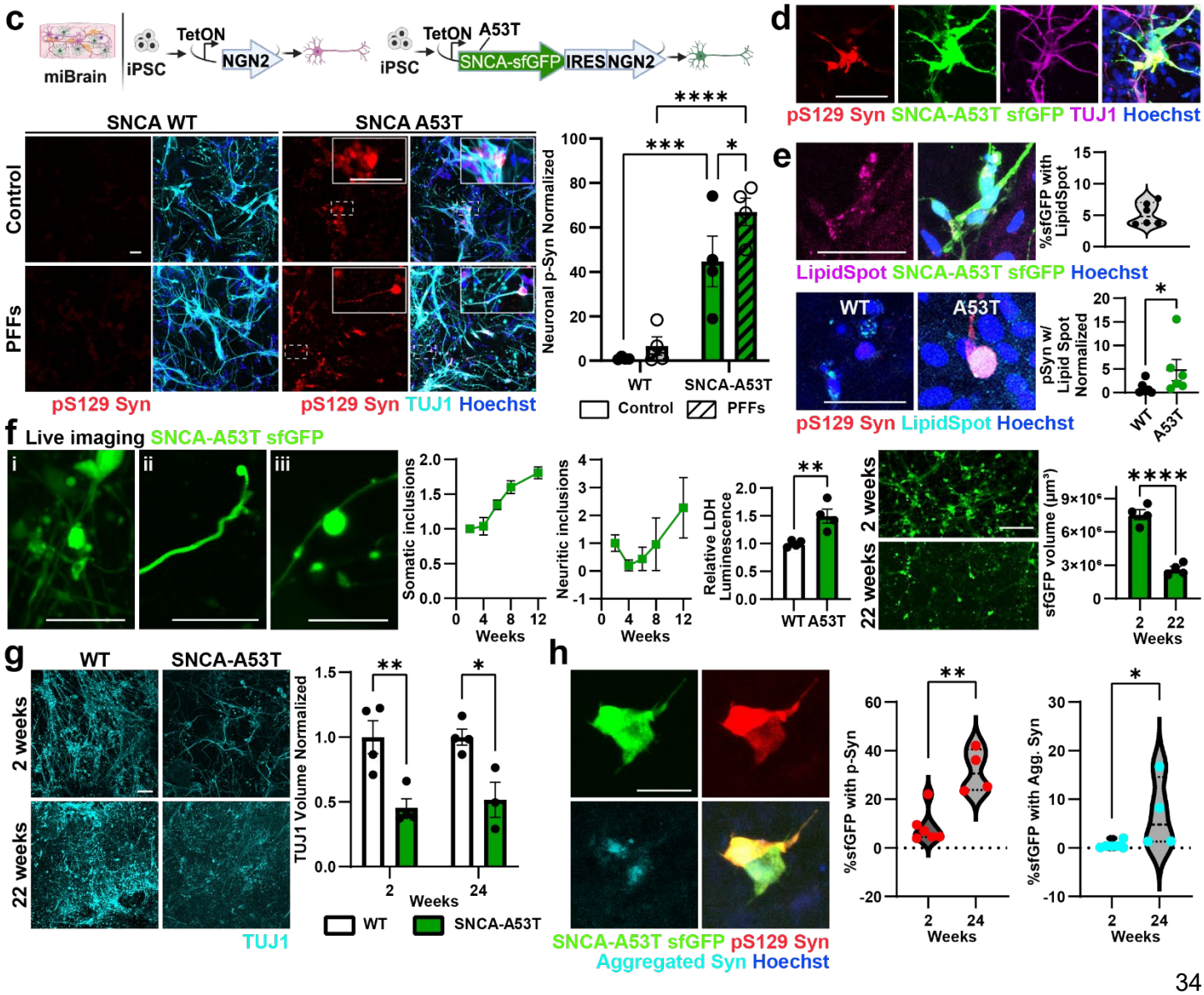

Figure 2

a

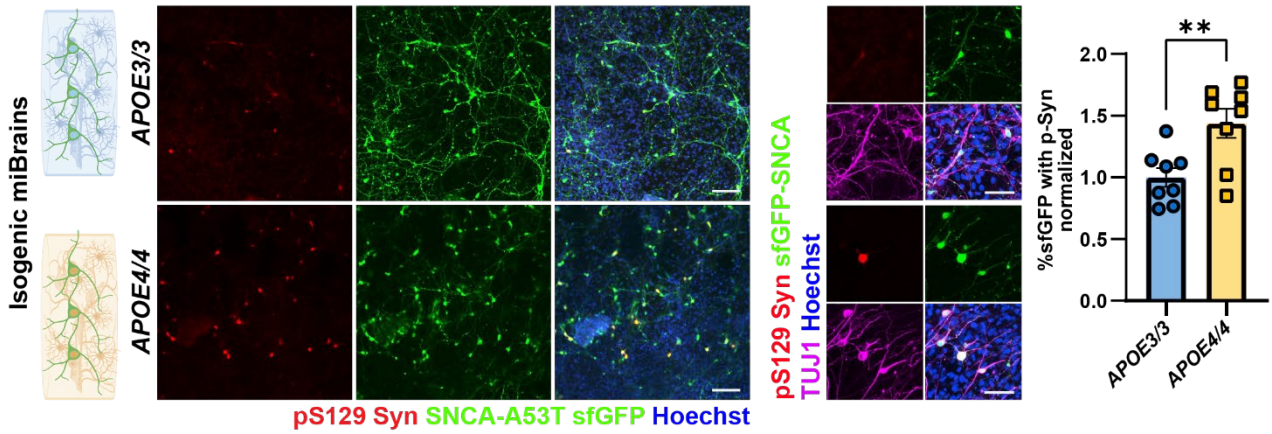
Isogenic miBrains
APOE3/3
APOE4/4
pS129 Syn SNCA-A53T sfGFP Hoechst
pS129 Syn sfGFP-SNCA
TUJ1 Hoechst
%sfGFP with p-Syn normalized
**
2.0
1.5
1.0
0.5
0.0
APOE3/3
APOE4/4

b

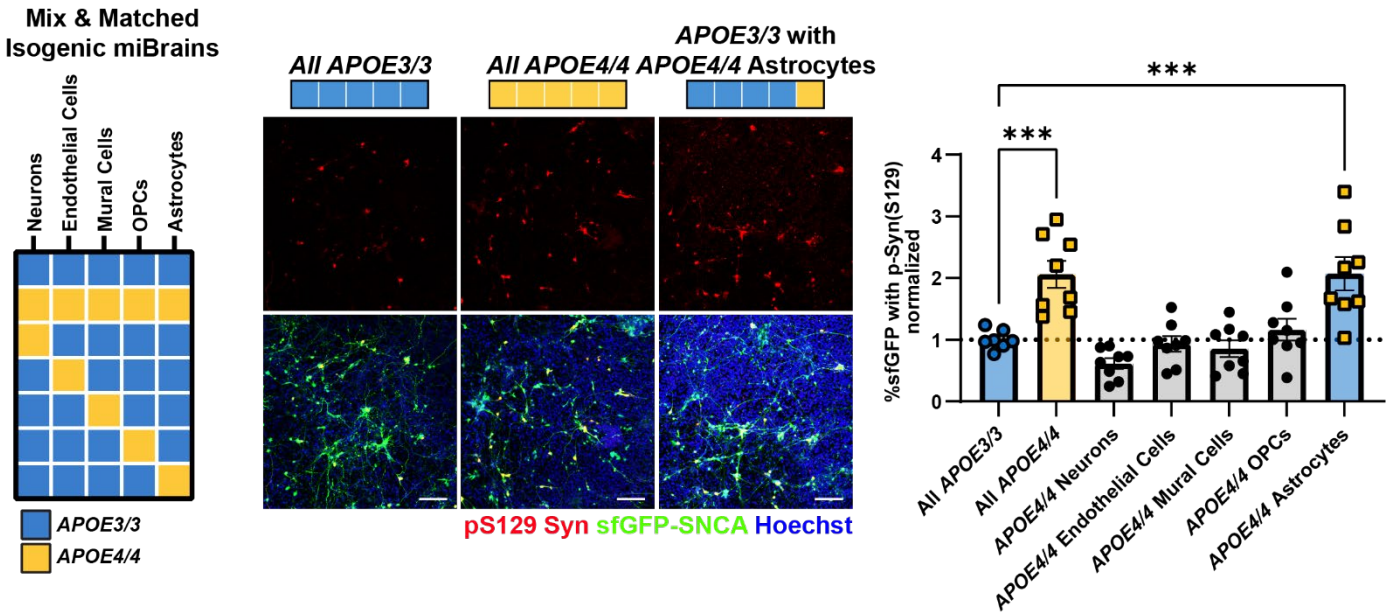
Mix & Matched Isogenic miBrains
Neurons
Endothelial Cells
Mural Cells
OPCs
Astrocytes
APOE3/3
APOE4/4
All APOE3/3
All APOE4/4
APOE3/3 with APOE4/4 Astrocytes
pS129 Syn sfGFP-SNCA Hoechst
%sfGFP with p-Syn(S129) normalized
***
***
4
3
2
1
0
All APOE3/3
All APOE4/4
APOE4/4 Neurons
APOE4/4 Endothelial Cells
APOE4/4 Mural Cells
APOE4/4 OPCs
APOE4/4 Astrocytes

c

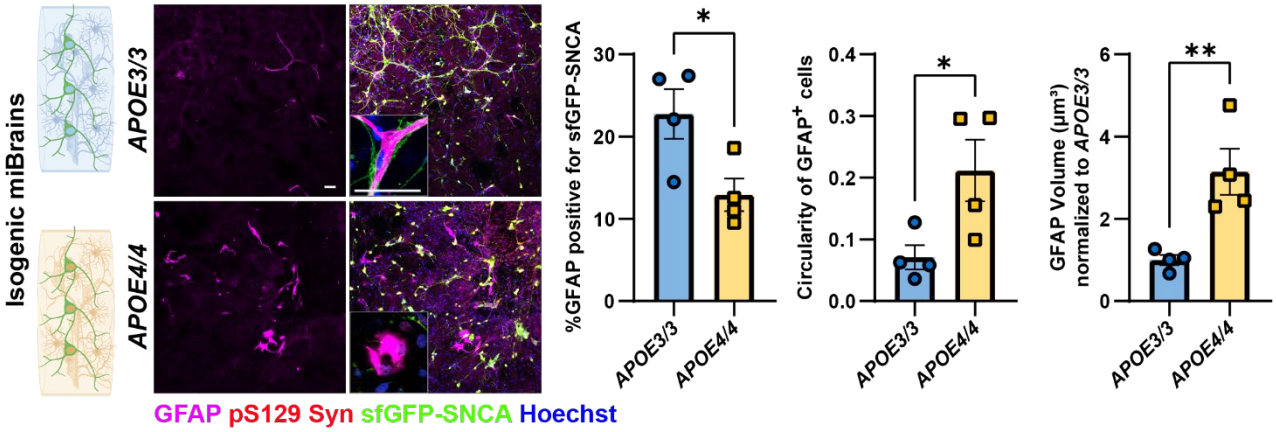
Isogenic miBrains
APOE3/3
APOE4/4
GFAP pS129 Syn sfGFP-SNCA Hoechst
%GFAP positive for sfGFP-SNCA
*
30
20
10
0
Circularity of GFAP+ cells
*
0.4
0.3
0.2
0.1
0.0
GFAP Volume (µm³) normalized to APOE3/3
**
6
4
2
0
APOE3/3
APOE4/4

Figure 3

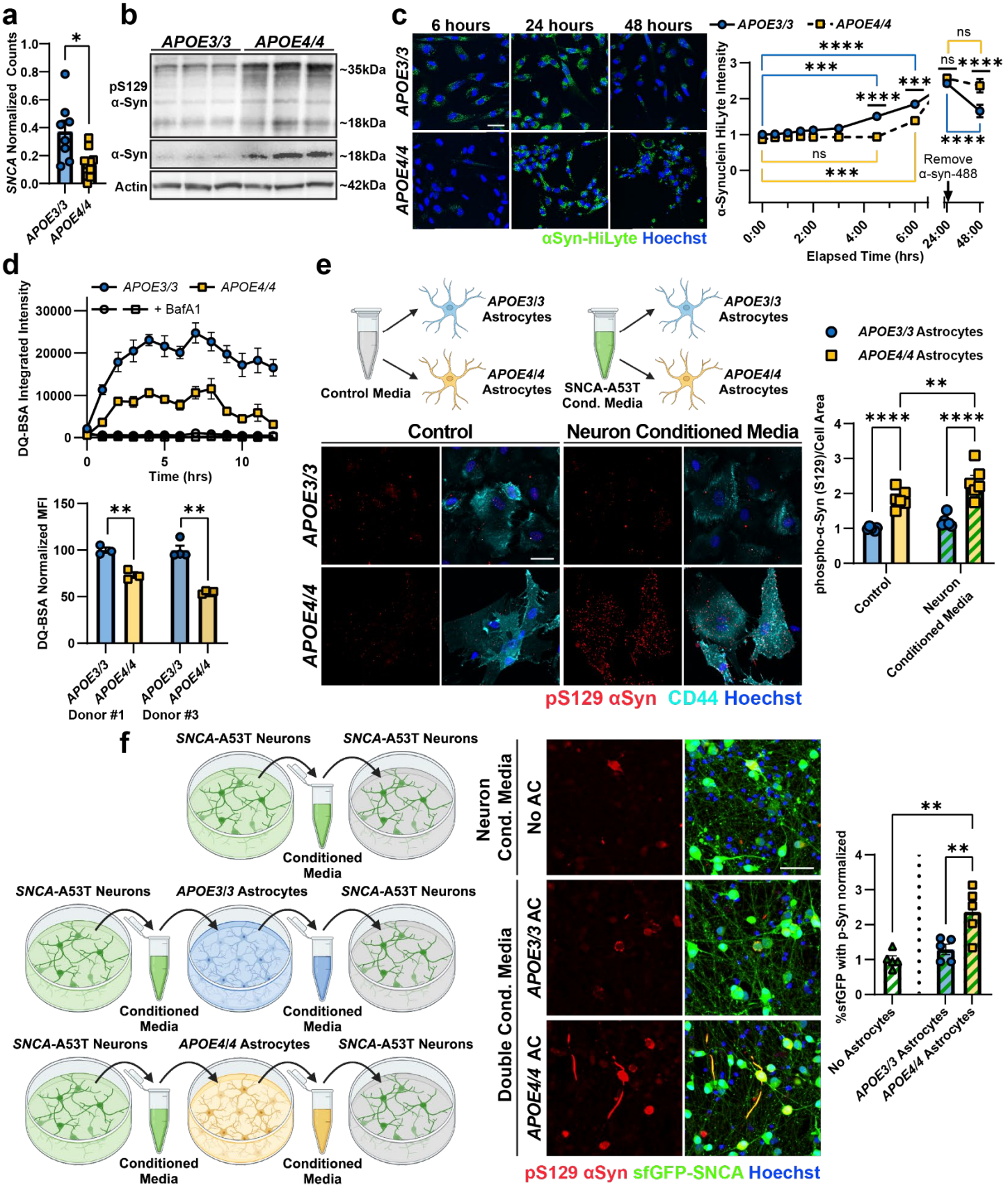
a
SNCA Normalized Counts
APOE3/3
APOE4/4
b
APOE3/3
APOE4/4
pS129 α-Syn
α-Syn
Actin
~35kDa
~18kDa
~18kDa
~42kDa
c
6 hours
24 hours
48 hours
APOE3/3
APOE4/4
αSyn-HiLyte Hoechst
α-Synuclein HiLyte Intensity
Elapsed Time (hrs)
Remove α-syn-488
d
APOE3/3
APOE4/4
+ BafA1
DQ-BSA Integrated Intensity
Time (hrs)
DQ-BSA Normalized MFI
Donor #1
Donor #3
e
Control Media
SNCA-A53T Cond. Media
APOE3/3 Astrocytes
APOE4/4 Astrocytes
Control
Neuron Conditioned Media
pS129 αSyn CD44 Hoechst
phospho-α-Syn (S129)/Cell Area
Control
Neuron Conditioned Media
f
SNCA-A53T Neurons
Conditioned Media
APOE3/3 Astrocytes
APOE4/4 Astrocytes
Neuron Cond. Media
No AC
Double Cond. Media
APOE3/3 AC
APOE4/4 AC
pS129 αSyn sfGFP-SNCA Hoechst
%sfGFP with p-Syn normalized
No Astrocytes
APOE3/3 Astrocytes
APOE4/4 Astrocytes

Figure 4

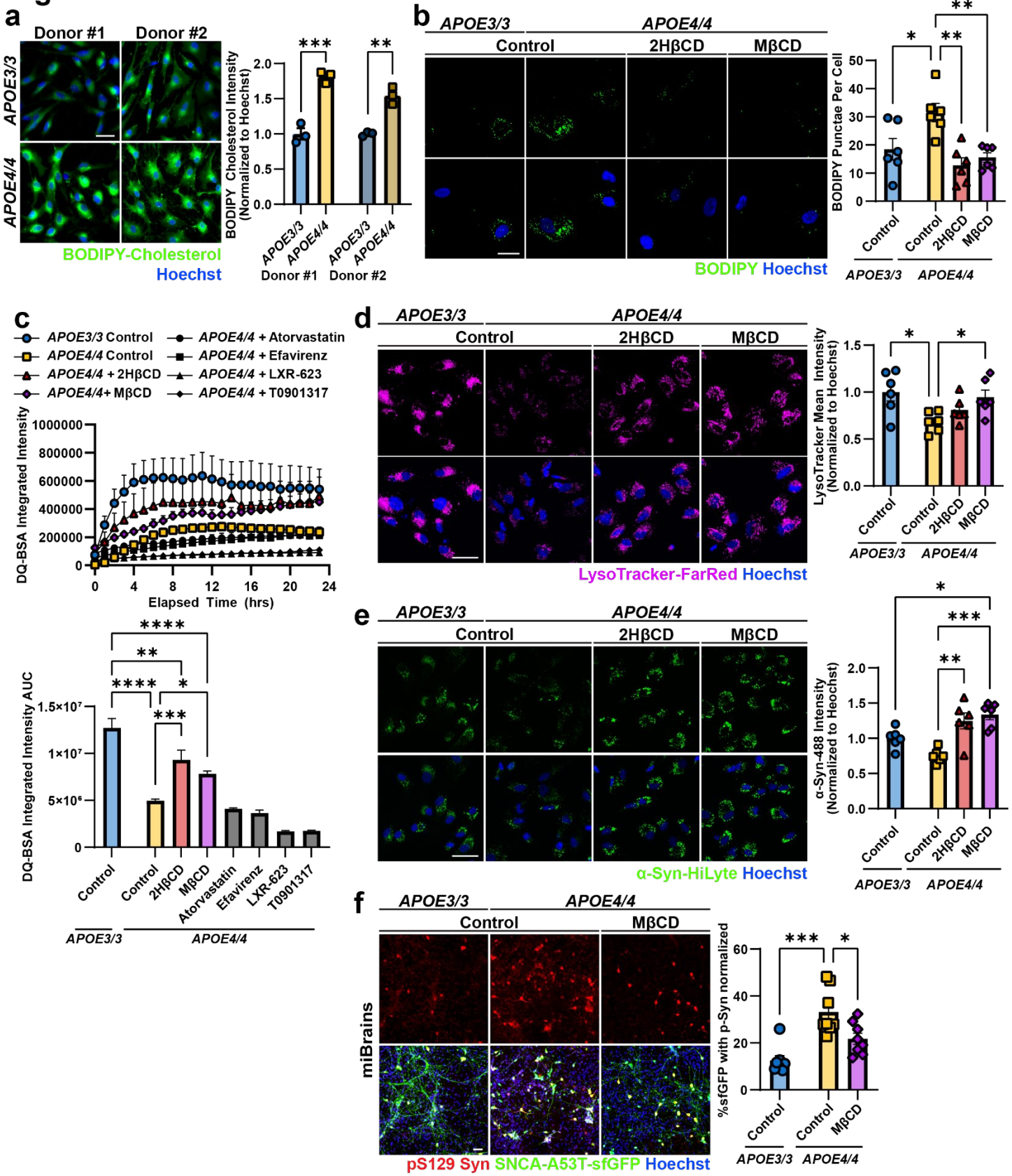
a
Donor #1
Donor #2
APOE3/3
APOE4/4
BODIPY-Cholesterol
Hoechst
BODIPY Cholesterol Intensity (Normalized to Hoechst)
APOE3/3
APOE4/4
Donor #1
Donor #2
b
APOE3/3
APOE4/4
Control
2HβCD
MβCD
BODIPY Hoechst
BODIPY Punctae Per Cell
Control
2HβCD
MβCD
c
APOE3/3 Control
APOE4/4 Control
APOE4/4 + 2HβCD
APOE4/4+ MβCD
APOE4/4 + Atorvastatin
APOE4/4 + Efavirenz
APOE4/4 + LXR-623
APOE4/4 + T0901317
DQ-BSA Integrated Intensity
Elapsed Time (hrs)
DQ-BSA Integrated Intensity AUC
Control
2HβCD
MβCD
Atorvastatin
Efavirenz
LXR-623
T0901317
d
LysoTracker-FarRed Hoechst
LysoTracker Mean Intensity (Normalized to Hoechst)
e
α-Syn-HiLyte Hoechst
α-Syn-488 Intensity (Normalized to Heochst)
f
miBrains
pS129 Syn SNCA-A53T-sfGFP Hoechst
%sfGFP with p-Syn normalized

Extended Data Fig. 1

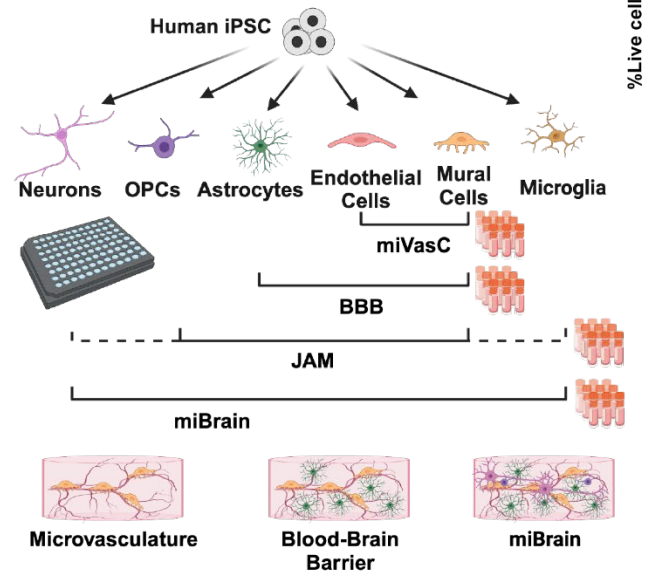

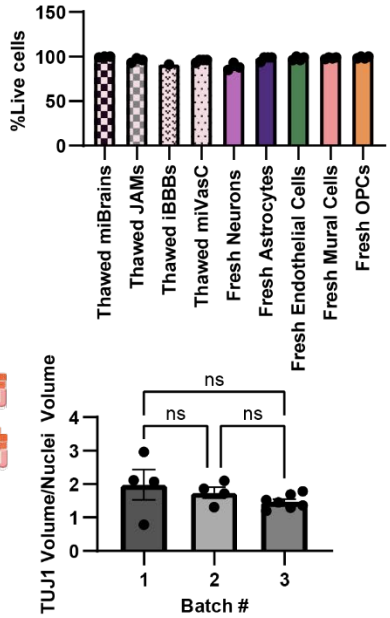

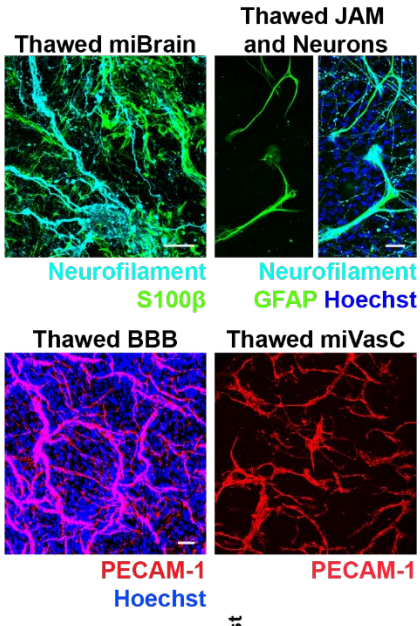

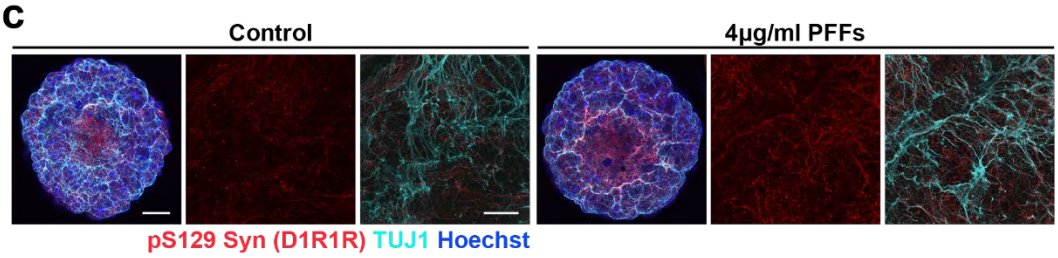

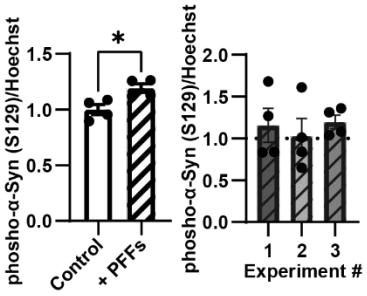

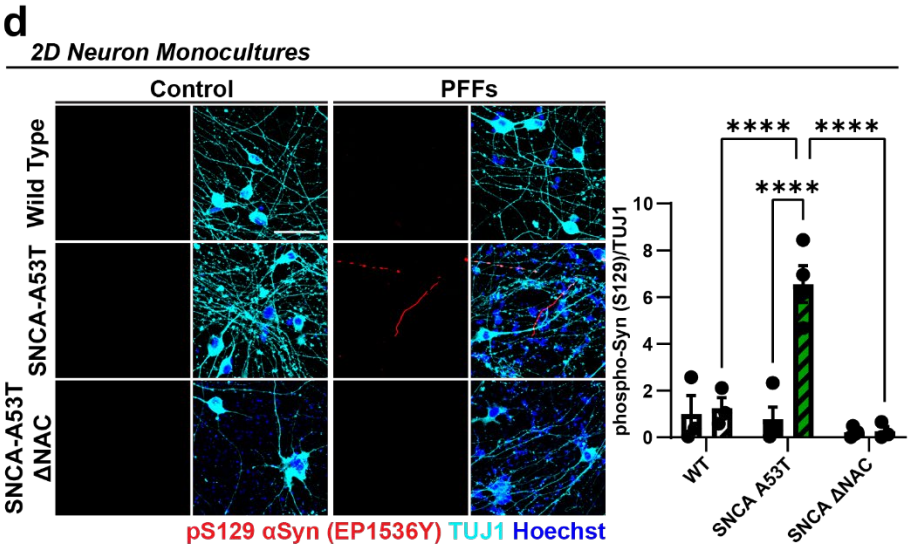

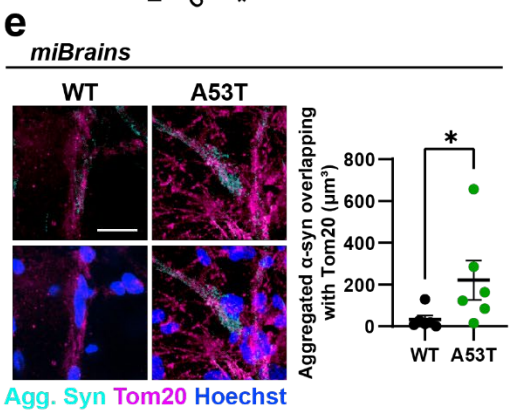

Extended Data Fig. 2

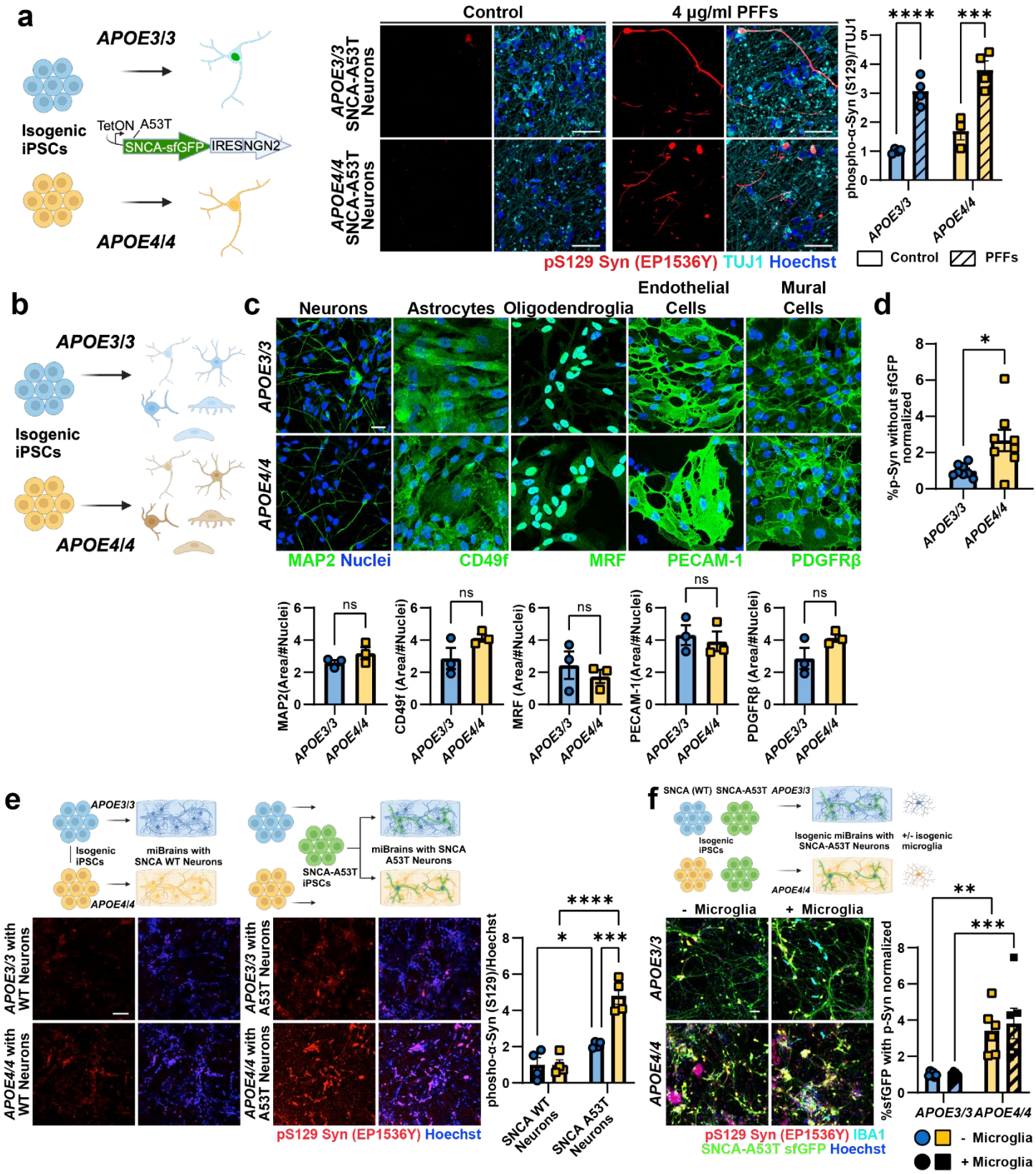

Extended Data Fig. 3

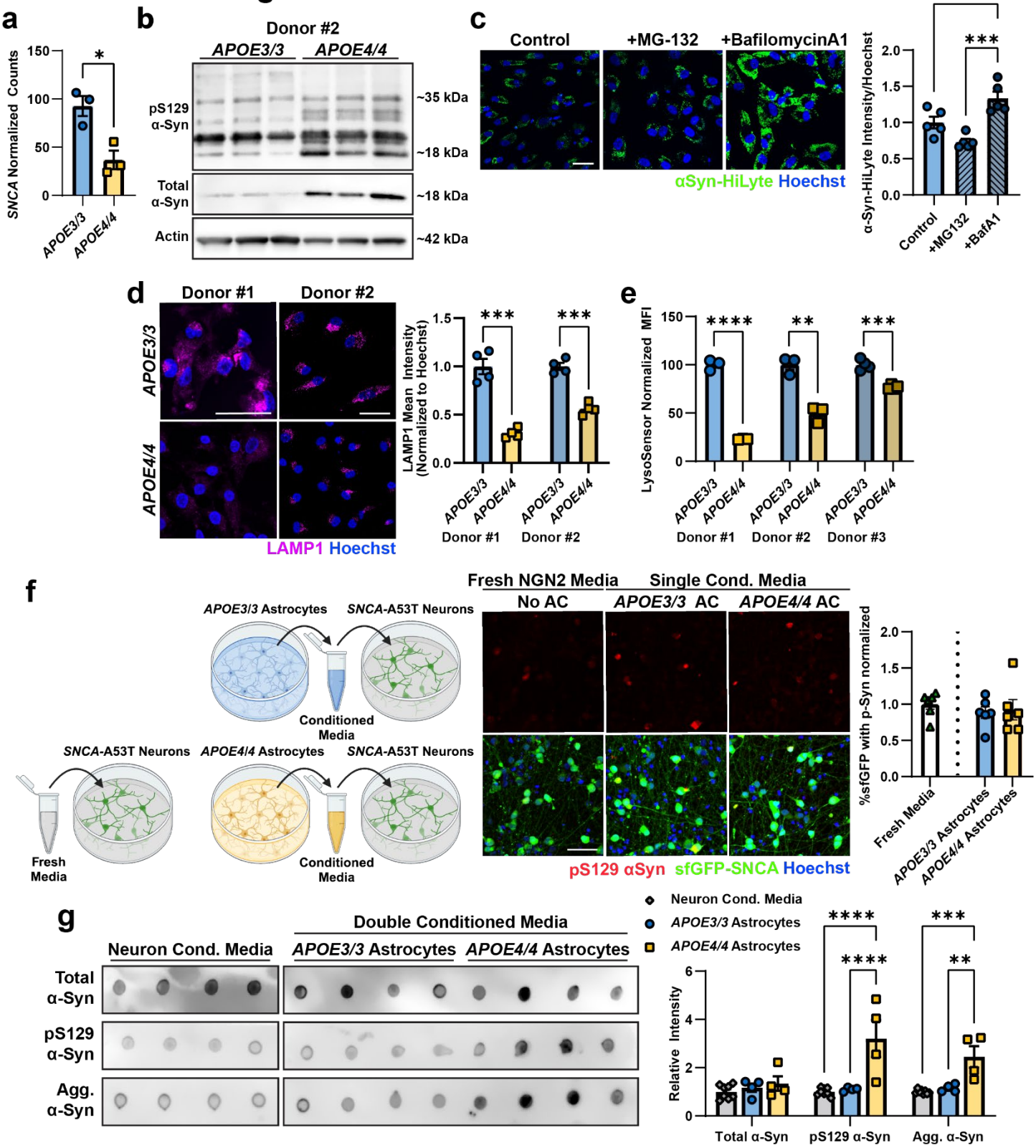
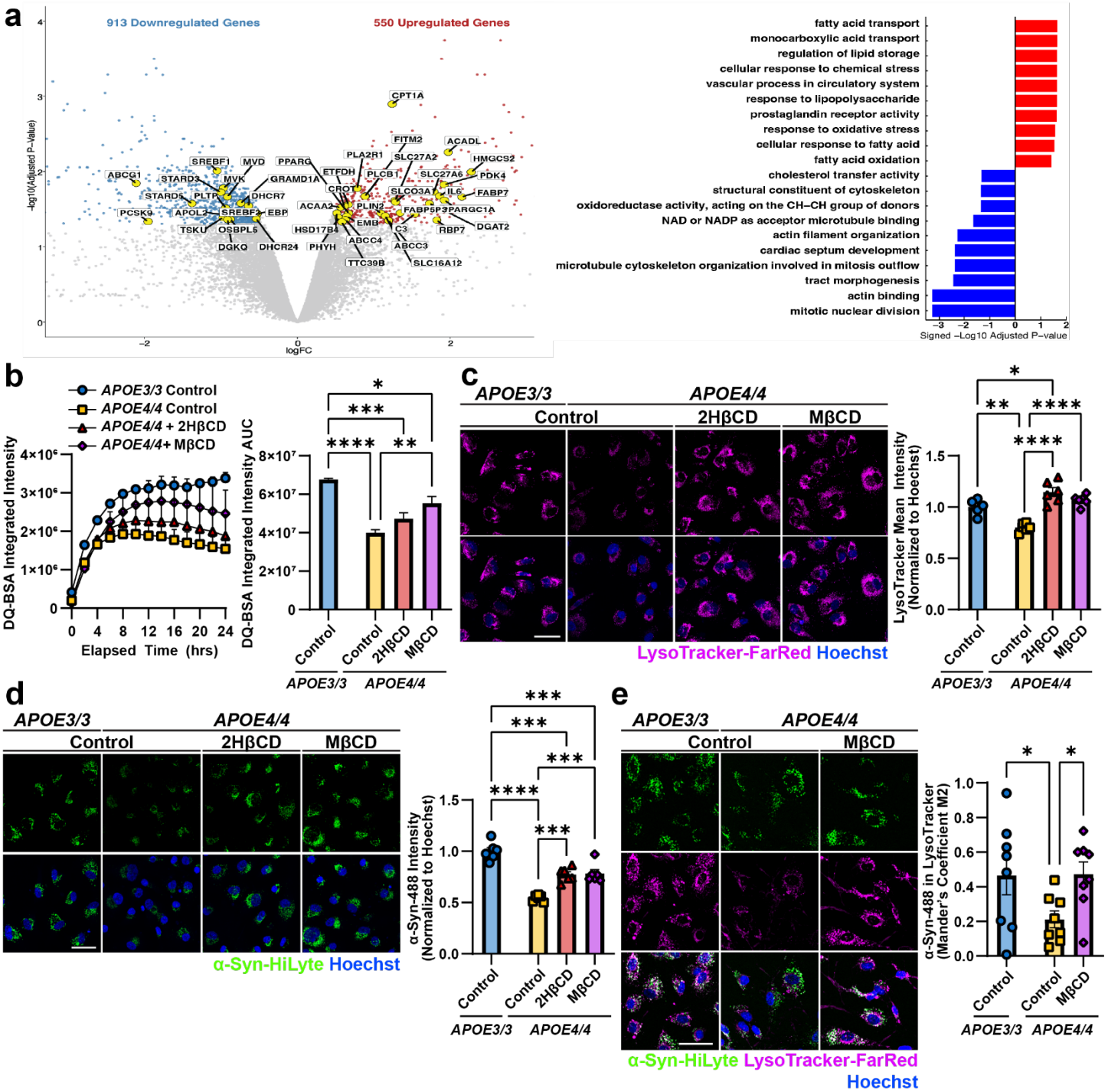
Extended Data Fig. 4